Article

Cell Chemical Biology

Dipyridamole Inhibits Lipogenic Gene Expression by Retaining SCAP-SREBP in the Endoplasmic Reticulum

Graphical Abstract

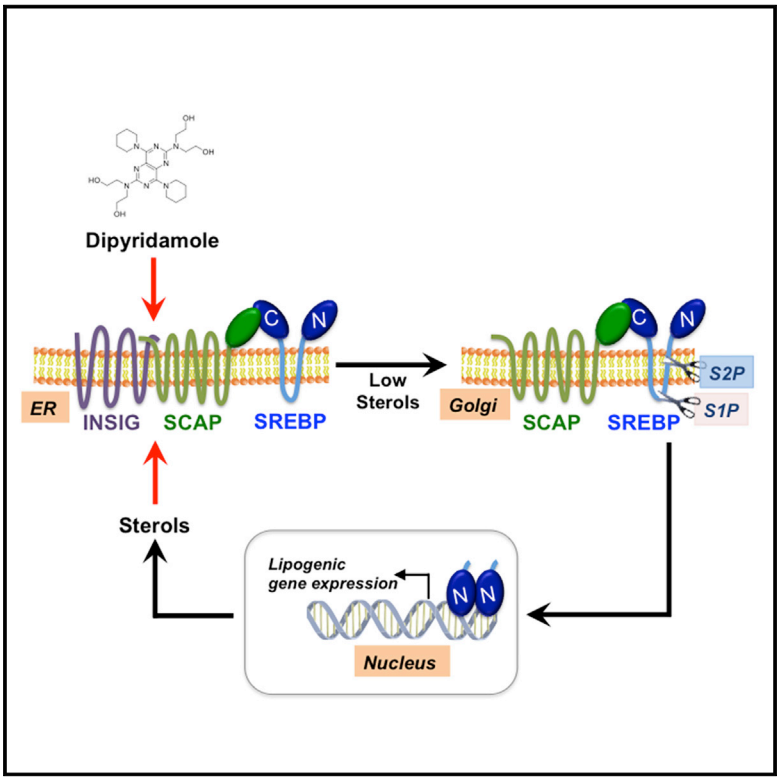

Highlights

- Dipyridamole, a PDE inhibitor, decreases lipogenesis by inhibiting SREBP maturation
- Dipyridamole blocks SREBP independent of its PDE inhibitory action
- A clickable photoprobe dipyridamole derivative binds to INSIG and SCAP
- Dipyridamole derivatives are potentially therapeutic for lipid disorders

Authors

Ryan M. Esquejo,
Manuel Roqueta-Rivera, Wei Shao, ...,
Carolyn E. Machamer,
Peter J. Espenshade,
Timothy F. Osborne

Correspondence

tosborn9@jhmi.edu

In Brief

Esquejo et al. report that dipyridamole, an FDA-approved anti-thrombotic phosphodiesterase (PDE) inhibitor, impedes endoplasmic reticulum to Golgi trafficking of sterol regulatory element-binding proteins (SREBPs) preventing their activation. A chemically modified version of dipyridamole that has no effect on PDE remains effective at SREBP blockage.

Esquejo et al., 2021, Cell Chemical Biology *28*, 169–179
February 18, 2021
https://doi.org/10.1016/j.chembiol.2020.10.003

CellPress

Cell Chemical Biology

CellPress

Article

Dipyridamole Inhibits Lipogenic Gene Expression by Retaining SCAP-SREBP in the Endoplasmic Reticulum

Ryan M. Esquejo,[1,7] Manuel Roqueta-Rivera,[1] Wei Shao,[2] Peter E. Phelan,[1] Uthpala Seneviratne,[3] Christopher W. am Ende,[4] Paul M. Hershberger,[5] Carolyn E. Machamer,[2] Peter J. Espenshade,[2] and Timothy F. Osborne[1,6,8,*]

[1]Sanford Burnham Prebys Medical Discovery Institute, Orlando, FL 32827, USA
[2]Department of Cell Biology, Johns Hopkins University School of Medicine, Baltimore, MD 21205, USA
[3]Chemical Biology and Medicine Design, Pfizer Inc, Cambridge, MA 02139, USA
[4]Pfizer Worldwide Research & Development, Eastern Point Road, Groton, CT 06340, USA
[5]Conrad Prebys Center for Chemical Genomics, Sanford Burnham Prebys Medical Discovery Institute, La Jolla, CA 92037, USA
[6]Present address: Institute for Fundamental Biomedical Research, Departments of Medicine and Biological Chemistry, Johns Hopkins University School of Medicine, St. Petersburg, FL 33701, USA
[7]Present address: Internal Medicine Research Unit, Pfizer Inc, Cambridge, MA 02139, USA
[8]Lead Contact
*Correspondence: tosborn9@jhmi.edu
https://doi.org/10.1016/j.chembiol.2020.10.003

SUMMARY

Sterol regulatory element-binding proteins (SREBPs) are master transcriptional regulators of the mevalonate pathway and lipid metabolism and represent an attractive therapeutic target for lipid metabolic disorders. SREBPs are maintained in the endoplasmic reticulum (ER) in a tripartite complex with SREBP cleavage-activating protein (SCAP) and insulin-induced gene protein (INSIG). When new lipid synthesis is required, the SCAP-SREBP complex dissociates from INSIG and undergoes ER-to-Golgi transport where the N-terminal transcription factor domain is released by proteolysis. The mature transcription factor translocates to the nucleus and stimulates expression of the SREBP gene program. Previous studies showed that dipyridamole, a clinically prescribed phosphodiesterase (PDE) inhibitor, potentiated statin-induced tumor growth inhibition. Dipyridamole limited nuclear accumulation of SREBP, but the mechanism was not well resolved. In this study, we show that dipyridamole selectively blocks ER-to-Golgi movement of the SCAP-SREBP complex and that this is independent of its PDE inhibitory activity.

INTRODUCTION

Lipids are essential building blocks of cell membranes, and they are also involved in a myriad and diverse collection of cellular functions that rely on a combination of their distinctive chemical features combined with their overall hydrophobic character. However, the overaccumulation of lipids results in hyperlipidemia and obesity, which can have deleterious health consequences. A recent CDC report shows that ~40% of adults in the US are considered obese, which poses medical as well as economic hardships on society (https://www.cdc.gov/obesity/data/adult.html). Hypercholesterolemia and hyperlipidemia are related to other metabolic diseases, such as hepatic steatosis, type 2 diabetes mellitus, cardiovascular disease, stroke, neurodegenerative disorders, and cancer (https://www.cdc.gov/cholesterol/index.htm).

The sterol regulatory element-binding proteins (SREBPs) are master regulators of lipid synthesis and regulate the expression of genes that code for many, if not all, of the enzymes required to synthesize triglycerides and cholesterol. There are three isoforms of SREBPs; SREBP-1a and SREBP-1c are splice variants that are derived from the *SREBF1* gene (Shimomura et al., 1997; Yokoyama et al., 1993), while SREBP-2 is expressed from the unlinked *SREBF2* gene (Hua et al., 1993). SREBPs are membrane bound transcription factors that are found in the endoplasmic reticulum (ER) where they associate with the SREBP cleavage-activating protein (SCAP) (Sakai et al., 1997), which contains a sterol-sensing domain that binds cholesterol directly (Adams et al., 2004; Radhakrishnan et al., 2004). The interaction between SCAP and a third ER resident protein, insulin-induced gene (INSIG), is favored when SCAP binds cholesterol and the association with INSIG anchors the SCAP-SREBP complex in the ER membrane (Adams et al., 2004; Yang et al., 2002). When intracellular sterol levels decline and SCAP binding to cholesterol is no longer favored, SCAP undergoes a conformational change that decreases its association with INSIG (Yang et al., 2002). Once released from this anchor, SCAP is picked up by the COPII vesicle trafficking complex, which carries the SCAP-SREBP complex to the Golgi

apparatus. The N-terminal transcription factor domain of SREBP is cleaved at two distinct sites by two Golgi membrane-localized proteases, site-1 protease (S1P) and site-2 protease (S2P) (Rawson et al., 1997; Sakai et al., 1996). The N-terminal portion of SREBP is located on the cytoplasmic face of the membrane and contains the sequence of the mature transcription factor. Proteolysis releases a cytoplasmic soluble mature SREBP (Sakai et al., 1996) that is targeted to the nucleus where it recognizes sterol regulatory element DNA sequences and promotes transcription of SREBP target genes (Horton et al., 2002).

Increased SREBP activity is associated with hepatic steatosis in both animal metabolic disease models and in humans, and targeting SREBP in mouse models can attenuate the associated fatty liver. For example, hamsters fed a high sucrose diet develop fatty liver due to increased hepatic SREBP-1c (Moon et al., 2012). The fatty liver was reversed by small interfering RNA (siRNA) targeting SCAP, which decreased nuclear SREBP levels (Moon et al., 2012). Interestingly, when mated with SREBP-1c knockout mice the fatty liver was resolved; however, there was no effect on overall obesity (Moon et al., 2012). Also, leptin-deficient *ob/ob* mice have increased hepatic SREBP-1c along with fatty liver (Shimomura et al., 1999). In contrast, treating mice with fatostatin or betulin, two small molecules shown to limit SCAP-SREBP migration from the ER to the Golgi apparatus, also reduces body weight in *ob/ob* (Kamisuki et al., 2009) or in wild-type mice fed a high fat diet (Tang et al., 2011), respectively. Thus, there is potential discordance in genetic and pharmacologic targeting of the SCAP, suggesting that the two drugs may have additional targets in addition to limiting SREBP nuclear accumulation.

There has also been some interest in targeting the mevalonate pathway in cancer, and statins have exhibited anticancer potential in several settings. However, the magnitude of the effect varies and the mechanism(s) of action have not been determined. In one study, investigators screened an FDA-approved drug library for compounds that would potentiate the minor effect of statins on growth of tumor cells in culture (Pandyra et al., 2014). One compound that significantly enhanced statin-dependent inhibition of tumor cell growth in culture and in a xenograft model was dipyridamole (Pandyra et al., 2014). Dipyridamole is an FDA-approved drug that inhibits platelet aggregation and is an effective anti-blood-clotting agent (Kim and Liao, 2008), so its synergy with statins was unexpected. Studies showed that dipyridamole might limit the nuclear accumulation of SREBP (Longo et al., 2019; Pandyra et al., 2014), but the specificity and mechanism of action were not determined.

In this study, we performed multiple *in vitro* and *in vivo* experiments to evaluate the effects of dipyridamole on SREBP. Our results show that dipyridamole targets SCAP-INSIG action in the ER to limit SREBP trafficking to the Golgi apparatus. We also show that these effects are independent of dipyridamole's PDE inhibitory action and are selective as dipyridamole had no effect on ER-to-Golgi movement of non-related cargo.

RESULTS

Dipyridamole Inhibits Nuclear Translocation and Activity of SREBP

Cholesterol and 25-hydroxycholesterol (25OH) interact with SCAP or INSIG, respectively, to limit translocation of the SCAP-SREBP complex from the ER-to-Golgi thereby preventing SREBP nuclear accumulation and limiting SREBP-dependent transcriptional programs (Adams et al., 2004; Radhakrishnan et al., 2004, 2007). In contrast, statin inhibition of HMG-CoA reductase decreases *de novo* sterol production, which reduces cholesterol for binding to SCAP and promotes SREBP maturation resulting in an increase in SREBP-dependent gene expression, which in turn promotes pathway flux. The compensatory increase in SREBP action can partially limit the effectiveness of statins and also promote non-lipid pathway actions of SREBPs. Therefore, two-pronged approaches that combine statins with compounds that limit SREBP maturation might have dual therapeutic advantages: to increase statin efficacy and to limit unwanted actions of increased nuclear SREBPs. A previous report by Penn and colleagues (Pandyra et al., 2014) showed that dipyridamole might prove effective in limiting the statin-associated increase in nuclear SREBP and increase the potency of statins in the inhibition of tumor growth. To evaluate this more directly and to uncover a potential mechanism, we incubated HeLa cells in lipoprotein-deficient medium supplemented with sterols, atorvastatin, or atorvastatin with increasing concentrations of dipyridamole. We found that dipyridamole reversed the effects of lipid depletion and atorvastatin on nuclear SREBP in a concentration-dependent manner (Figure 1B). This was paralleled by a similar decrease in expression of known SREBP target genes, such as *HMGCR* and *FASN* (Figures 1C and 1D). We also used an antibody that recognizes the N-terminal region of SREBP-2 in *in vitro* immunolocalization studies, which showed that dipyridamole, similar to sterols, prevented SREBP-2 nuclear accumulation (Figure 1E). In the absence of an exogenous source of cholesterol, CHO-7 cells require the SREBP pathway for growth (Hua et al., 1996; Metherall et al., 1989; Yabe et al., 2002). We found that dipyridamole suppressed the growth of CHO-7 cells only when cultured in the absence of cholesterol (Figure 1F). These data suggest that the main growth inhibitory effects of dipyridamole are on lipid accumulation through the SREBP pathway.

SREBP-driven lipid synthesis is robust in the mammalian liver when animals are fed a carbohydrate-enriched diet after a prolonged fast (Horton et al., 1998). Consistent with this, nuclear SREBPs are low during fasting, and they rapidly accumulate in hepatic nuclei during the refeeding phase (Horton et al., 1998). To determine whether dipyridamole might affect nuclear SREBPs *in vivo*, we performed a fasting/refeeding experiment in which one cohort was injected with dipyridamole at the time of refeeding, and nuclear SREBP-1 and SREBP-2 were monitored by immunoblotting. We intraperitoneally dosed mice with either 40 or 120 mg/kg dipyridamole and found that 120 mg/kg effectively limited the refeeding-associated nuclear accumulation of both SREBP-1 and SREBP-2 (Figures S1A and 1G). Dipyridamole had no effect on the phosphorylation of AKT and ribosomal S6 proteins during refeeding, suggesting that dipyridamole did not have a broader effect on the major insulin receptor-mediated signaling pathway (Figure S1B). We also found that dipyridamole significantly suppressed the hepatic expression of SREBP target genes, such as *Hmgcr*, *Fasn*, and *Insig1* compared with refed animals that received vehicle (Figure 1H). We did not find a significant difference in the expression of genes that are known to be induced by fasting and repressed by

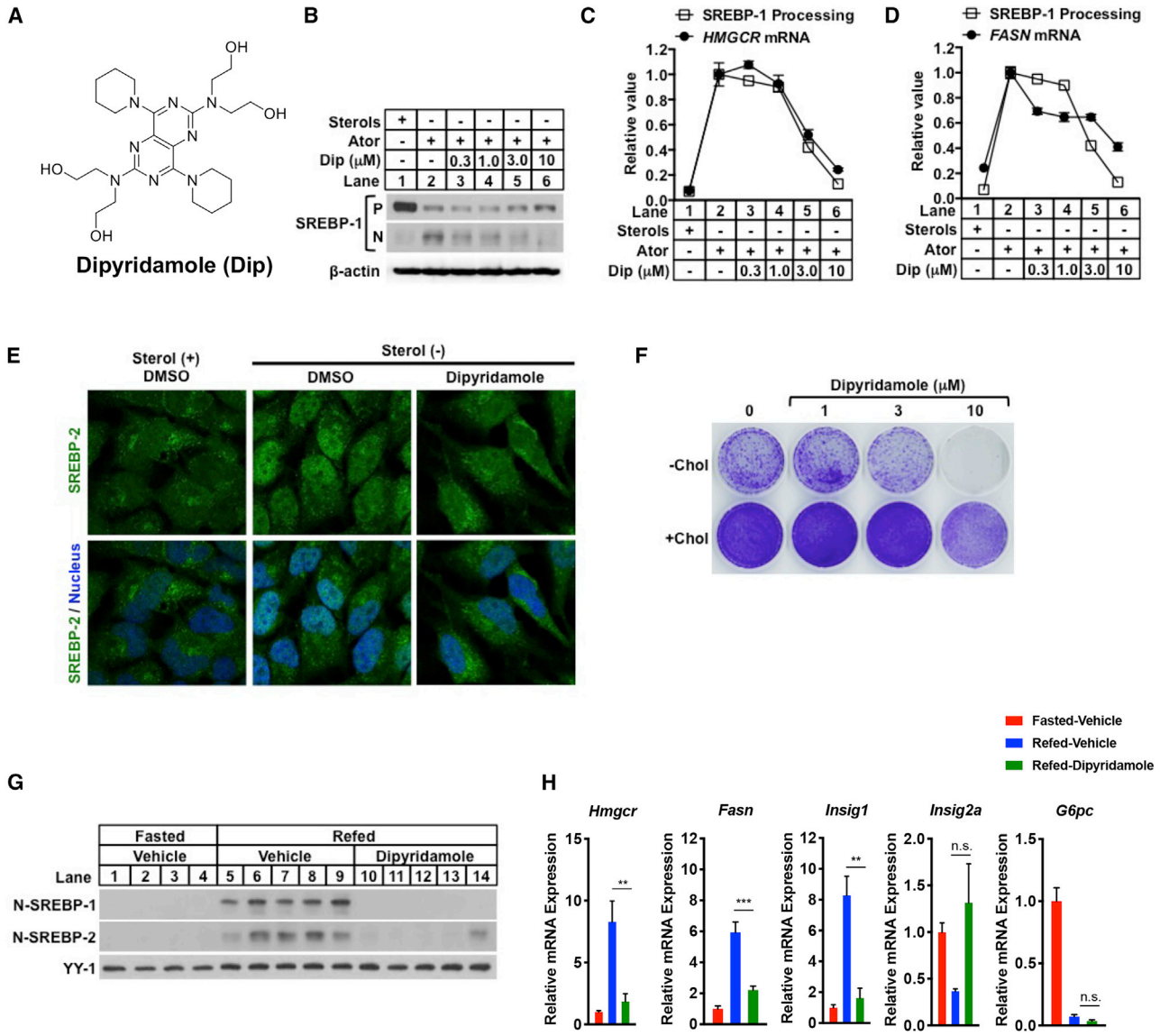

Figure 1. Dipyridamole Inhibits SREBP Maturation

(A) Dipyridamole structure.

(B–D) HeLa cells were incubated in DMEM with 5% lipoprotein-deficient serum (LPDS) containing sterols (12 μg/mL cholesterol and 1 μg/mL 25-OH cholesterol) or atorvastatin (Ator) (10 μM) with increasing concentrations of dipyridamole (Dip). (B) Immunoblots for precursor and nuclear forms of SREBP-1 and β-actin from HeLa cell lysates. (C) *HMGCR* and *FASN* mRNA expression (black squares) and ratio of nuclear to precursor forms of SREBP-1 densitometry (open black squares). Gene expression data are from three biological replicates (mean ± SEM).

(E) Immunofluorescence images for SREBP-1 (green) and nuclei (blue) in HeLa cells after a 6-h incubation in medium with sterols or atorvastatin (10 μM) with and without dipyridamole (10 μM).

(F) Crystal violet staining of CHO-7 cells after 12 days in DMEM:F-12 (50:50) media with 5% LPDS and ± cholesterol with increasing concentrations of dipyridamole.

(G and H) Nine- to 13-week-old male mice were subjected to a fasting/refeeding experiment and dosed (i.p.) with either vehicle or dipyridamole (120 mg/kg) during the refeeding period as described in the STAR Methods. (G) Immunoblots for SREBP-1, SREBP-2, and YY-1 from liver nuclear fraction. (H) RNA expression for the indicated genes was measured by qPCR. Five to six animals were dosed in each group.

Error bars represent ± SEM. Unpaired Student's t test was used to evaluate statistical significance, $^{**}p < 0.01$, $^{***}p < 0.001$; n.s., not significant. See also Figure S1.

refeeding, such as *Insig2a* and *G6pc*, which together with the lack of effect on AKT signaling provides strong evidence that dipyridamole did not perturb the fundamental fasting/refeeding transition (Figure 1H).

Dipyridamole Retains the INSIG-SCAP-SREBP Complex in the ER

To determine more precisely how dipyridamole limits nuclear SREBP accumulation, we transfected HeLa cells with CMV

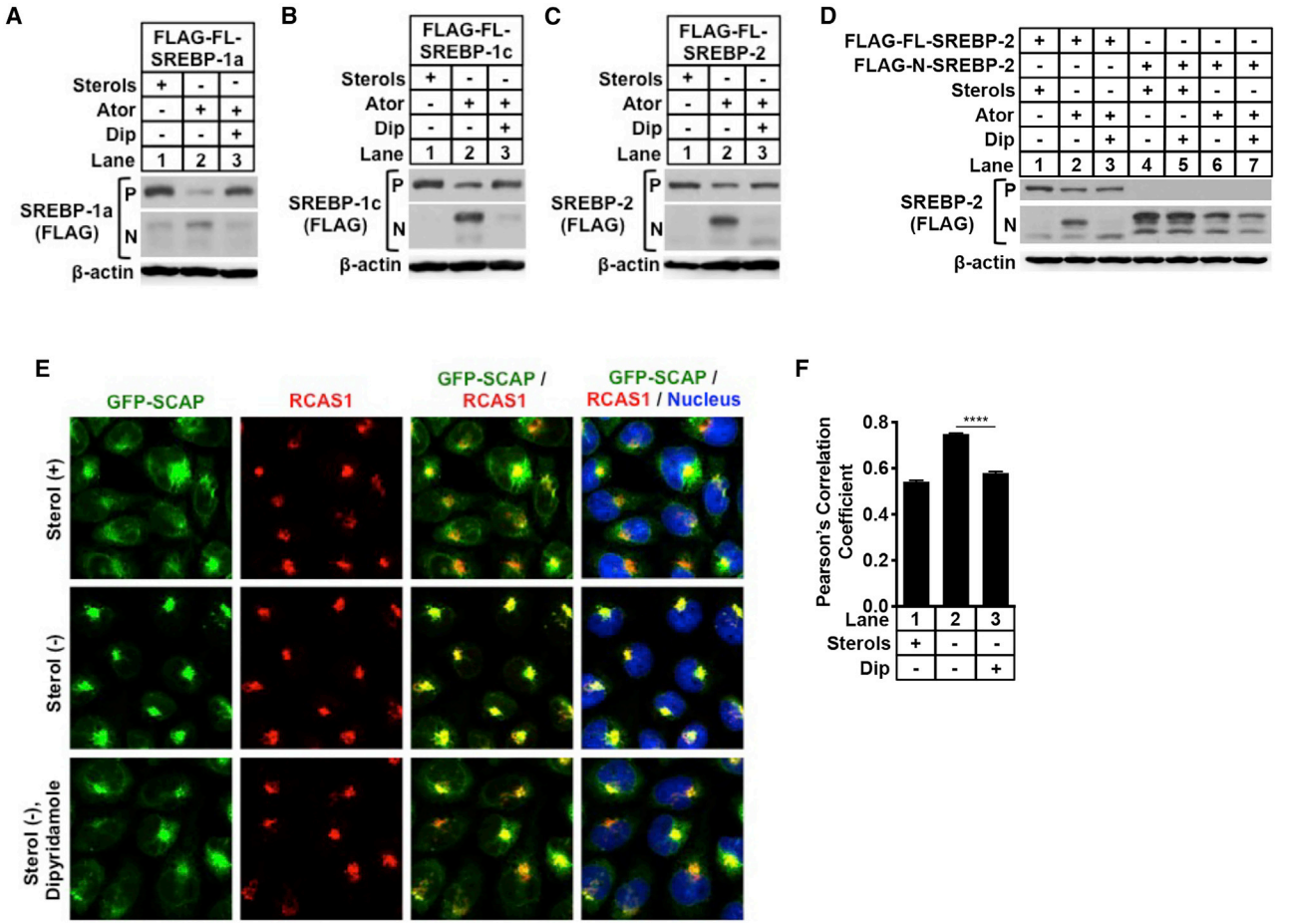

Figure 2. Dipyridamole Leads to Retention of INSIG-SCAP-SREBP Complex in the ER

(A–C) HeLa cells were transfected with plasmids expressing full-length SREBP-1a, SREBP-1c, or SREBP-2 with 3xFLAG sequence attached to the N-terminal end and then cultured in medium containing 5% LPDS with sterols or atorvastatin (Ator) ± dipyridamole (Dip) (10 μM). Immunoblots for precursor and mature SREBPs and β-actin are presented.

(D) HeLa cells were transfected with plasmids encoding either an N-terminal 3xFLAG-tagged full-length SREBP-2 as in (C) or a constitutively nuclear-targeted mature form of SREBP-2 with 2X-FLAG. Following culture in DMEM with 5% LPDS with sterols, atorvastatin (10 μM) and dipyridamole (10 μM) immunoblots were performed on cell extracts with antibodies detecting either FLAG or β-actin.

(E and F) CHO cells stably expressing GFP-tagged SCAP were grown in DMEM/F-12 medium supplemented with 5% lipoprotein-deficient serum, 1% hydroxypropyl-β-cyclodextrin (HPCD) with sterols or dipyridamole. (E) Confocal images of GFP-SCAP and Golgi marker RCAS1. (F) Pearson's correlation coefficient values for GFP-SCAP and RCAS1 co-localization (n = 100 cells/condition). Error bars represent ± SEM. Unpaired Student's t test was used to evaluate statistical significance, ****$p < 0.0001$.

promoter-driven expression constructs encoding N-terminal FLAG-tagged full-length SREBP-1a, SREBP-1c, or SREBP-2, followed by incubation in medium containing sterols, or sterol-depleted medium supplemented with atorvastatin, in the presence or absence of dipyridamole. Similar to our observation with endogenous SREBP, we found that cells treated with dipyridamole limited nuclear accumulation of FLAG-tagged SREBPs (Figures 2A–2C). These results suggest that dipyridamole decreases SREBP accumulation at a post-transcriptional step. In addition, dipyridamole had no effect on nuclear accumulation of SREBP from a human cytomegalovirus (CMV) promoter-driven expression vector that encodes the mature and constitutively nuclear-targeted form (Figure 2D). Combined together, these two observations suggest that dipyridamole affects SREBP at a step after gene transcription but before nuclear protein turnover, which includes the SCAP-INSIG-dependent ER-to-Golgi trafficking itinerary.

To directly evaluate whether dipyridamole alters the ER-to-Golgi trafficking of SCAP, we monitored the cellular location of a GFP-SCAP fusion protein in CHO-7 cells cultured in the absence or presence of sterols. GFP-SCAP preferentially co-localized with the RCAS1 Golgi marker protein when cells were cultured in the absence of sterols, and this association was reduced when dipyridamole was added (Figures 2E and 2F). This observation suggests that dipyridamole directly influences the ER-to-Golgi trafficking of SCAP.

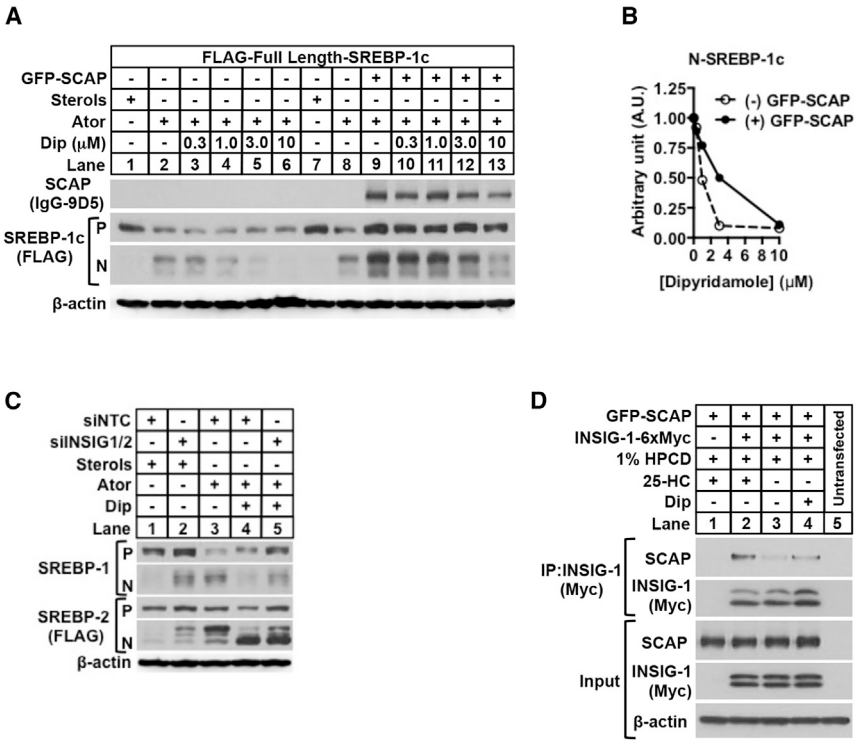

Figure 3. Dipyridamole Acts at the SCAP-INSIG Interaction Step to Block SREBP Maturation

(A and B) HeLa cells were co-transfected with plasmids expressing GFP-SCAP and N-terminal 3xFLAG-tagged SREBP-1c as indicated. Cells were incubated in DMEM containing 5% LPDS with sterols or atorvastatin (Ator) (10 μM) and where indicated an increasing concentration of dipyridamole (Dip) was included. (A) Immunoblots for SCAP (IgG-9D5), FLAG-tagged SREBP-1c, and β-actin. (B) Data in (A) were quantified and plotted relative to control values as indicated. This experiment is representative of three experiments.

(C) HeLa cells were co-transfected with N-terminal 3xFLAG-tagged full-length SREBP-2 and, where indicated, siRNAs against non-targeting control, INSIG1, and INSIG2 were included, after incubation in DMEM containing 5% LPDS with sterols or atorvastatin (10 μM) ± dipyridamole (10 μM) as indicated. Cells were harvested after 24 h and immunoblots for precursor and nuclear forms of SREBP-1 and FLAG-tagged SREBP-2, and β-actin were performed.

(D) HeLa cells were transfected with pCMV-GFP-SCAP and pCMV-INSIG-1-6xMyc and incubated in DMEM medium with 1% hydroxypropyl-β-cyclodextrin (HPCD) in the presence of 25-OH cholesterol and dipyridamole (10 μM) for 5 h. Cell extracts were subject to immunoprecipitation with Myc antibody followed by immunoblots for SCAP (IgG-9D5), Myc-tagged INSIG or β-actin as shown. See also Figure S2.

Dipyridamole Blocks SCAP-SREBP Complex ER-to-Golgi Trafficking by Promoting INSIG-SCAP Interaction

Because INSIG binding to SCAP is the critical event that anchors SREBPs in the ER, changing the ratio of SCAP to INSIG can also modulate the trafficking of SREBPs. If dipyridamole acts at the SCAP-INSIG interaction step to influence SREBP movement, then altering levels of SCAP or INSIG should also modify the effects of dipyridamole. SREBP nuclear accumulation was increased when SCAP was overexpressed, and its inclusion limited the inhibitory effects of dipyridamole (Figures 3A, 3B, S2A, and S2B). Conversely, when endogenous INSIG-1 and -2 were simultaneously reduced through siRNA targeting, the inhibitory effects of dipyridamole on nuclear accumulation of SREBP and SREBP target gene expression were also blunted (Figures 3C and S2C–S2F).

Artificial attachment of the KDEL ER retention signal to the site-1 protease (S1P) was shown to override the cholesterol suppression of SREBP processing (DeBose-Boyd et al., 1999). Co-transfection of the S1P-KDEL construct also blocked the effect of dipyridamole on SREBP nuclear accumulation (Figures S2G and S2H), and treatment of cells with brefeldin A, which results in ER accumulation of Golgi targeted proteins, had a similar effect (Figure S2I). Finally, when Myc-tagged INSIG-1 was immunoprecipitated from cells co-transfected with GFP-SCAP that were treated with dipyridamole, SCAP co-precipitation was enhanced similar to the effects of 25-OH cholesterol (Figure 3D).

Dipyridamole Stabilizes INSIG Protein

Based on these results, we hypothesized that dipyridamole likely affects levels of nuclear SREBP by acting through ER-to-Golgi trafficking steps involving INSIG and/or SCAP. INSIG proteins have a relatively short half-life and oxysterol binding stabilizes INSIG (Gong et al., 2006), which enhances its binding to SCAP and this contributes to ER retention of the SCAP-SREBP complex. To determine whether dipyridamole might act similarly, we measured the half-life of C-terminal Myc-tagged INSIG-1 expressed in cells treated with cycloheximide and then incubated with 25-OH cholesterol as a control or dipyridamole and followed expression of Myc-tagged INSIG-1 over time. Similar to 25-OH cholesterol, dipyridamole stabilized Myc-INSIG-1 (Figures 4A and 4B), but it had no effect on the rapid turnover of endogenous c-Myc, which reacts with the same antibody (Figures 4A and 4C). We also measured INSIG-2 in the membrane fractions (Figure 4D) during a fasting/refeeding where dipyridamole treatment in mice prevented the feeding-associated increase in nuclear SREBP levels (Figure 1G). These results show that injection of dipyridamole increased Insig-2 protein levels during refeeding (Figure 4D), which is a condition where *Insig2* mRNA levels normally decline. This *in vivo* result is also consistent with dipyridamole stabilizing Insig protein levels. .

Dipyridamole Inhibits SREBP Maturation Independent of cAMP/cGMP Signaling Pathways

Dipyridamole is a known phosphodiesterase (PDE) inhibitor capable of raising both intracellular cAMP or cGMP levels, which

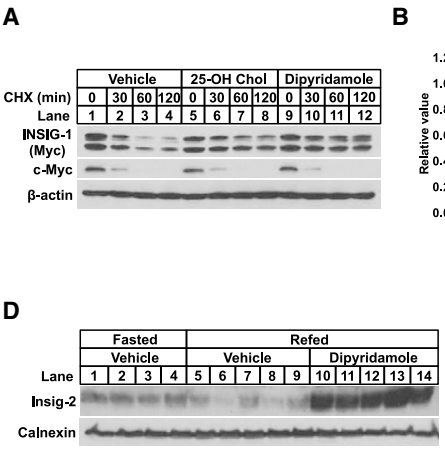

Figure 4. Dipyridamole Stabilizes INSIG Protein

(A) HeLa cells transfected with Myc-tagged INSIG-1 were incubated in DMEM with 5% LPDS and atorvastatin (Ator) (10 μM) overnight; the next day, cells were treated with cycloheximide (CHX) (50 μM) in the presence of vehicle, 25-OH cholesterol (1 μg/mL), or dipyridamole (Dip) (10 μM) and cells were harvested after the indicated incubation time and extracts were subjected to immunoblotting to detect Myc-tagged INSIG-1, c-Myc, and β-actin.

(B and C) Data in (A) were quantified and plotted relative to control values as indicated. This experiment is representative of two experiments. Error bars represent ± SEM.

(D) Membrane protein fractions prepared from the livers of male mice in the fast/refeeding experiment described in the legend to Figure 1 were used for immunoblots to detect either Insig-2 and calnexin.

results in activation of either protein kinase A (PKA) or protein kinase G, respectively (Kim and Liao, 2008). To determine whether dipyridamole suppresses SREBP maturation through a cAMP- or cGMP-dependent pathway, we treated HeLa cells with dipyridamole or forskolin, which is known to increase intracellular cAMP levels. We found that, unlike dipyridamole, forksolin did not suppress SREBP maturation in HeLa cells (Figure S3A). To further investigate the function cAMP signaling on SREBP processing, we incubated HeLa cells in medium with sterols, or in the absence of sterols plus atorvastatin supplemented with dipyridamole, forskolin and dipyridamole, or forskolin and 3-isobutyl-1-methylxanthine (IBMX), which is a non-selective PDE inhibitor. We found that, unlike dipyridamole, IBMX by itself or even in combination with forskolin did not suppress SREBP maturation even though these conditions increased phosphorylation of PKA substrates as measured by immunoblotting of cell extracts with an antibody recognizing PKA phosphorylation sites (Figure S3B). Given that PDE inhibitors can increase both cAMP and cGMP levels, we tested the effects of a cell-permeable cGMP molecule on SREBP processing in HeLa cells in sterol-depleted conditions in the presence of IBMX. We found that, unlike dipyridamole, cGMP with or without IBMX did not affect SREBP maturation (Figure S3C).

A Dipyridamole Analog that Selectively Inhibits SREBP Activity but Is Not a PDE Inhibitor

To begin to probe the structural features of dipyridamole involved in inhibiting SREBP maturation, we first converted the four free -OH groups of dipyridamole to -CH_3O generating a modified dipyridamole molecule (N2,N2,N6,N6-tetrakis[2-methoxyethyl]-4,8-di[piperidin-1-yl]pyrimido[5,4-d]pyrimidine-2,6-diamine, referred to here as TM-dipyridamole) (Figure 5A). We compared the effects of dipyridamole and TM-dipyridamole on SREBP maturation in HeLa cells and found that TM-dipyridamole was a more potent inhibitor of SREBP activity than the parental dipyridamole molecule (Figures 5B–5D). Interestingly, unlike dipyridamole, the conversion to TM-dipyridamole significantly reduced its ability to inhibit PDE activity (Figure S4A). TM-dipyridamole is more hydrophobic than dipyridamole, which limited our ability to perform long-term *in vivo* studies. However, in an acute fasting/refeeding experiment in mice, TM-dipyridamole prevented accumulation of nuclear SREBP-1 in the liver during refeeding (Figure S4B). TM-dipyridamole also blunted the expression of known SREBP targets, such as *Hmgcr*, *Fasn*, and *Insig1*, in the liver during refeeding. Meanwhile, TM-dipyridamole did not affect the expression of *Pck1* in the livers compared with vehicle-treated refed mice (Figures S4C–S4F). These results parallel those achieved with dipyridamole presented earlier (Figure 1H).

Consistent with results for dipyridamole (Figure 1F), TM-dipyridamole inhibited growth of CHO-7 cells in lipid-poor medium (Figure 5E). Addition of lipid bypassed the effect of TM-dipyridamole, indicating that, similar to dipyridamole, TM-dipyridamole affects lipid supply. Although the growth assay provides evidence that SREBP maturation is the major cellular event targeted by dipyridamole and TM-dipyridamole, these results do not address whether dipyridamole might also interfere with the general trafficking of other proteins from the ER to the Golgi. In fact, fatostatin, another small molecule that inhibits SREBP ER-to-Golgi trafficking (Kamisuki et al., 2009) also inhibits ER-to-Golgi trafficking of other non-related proteins (Shao et al., 2016). Fatostatin is therefore not selective for the SREBP pathway. To determine whether TM-dipyridamole broadly inhibits ER-to-Golgi transport, we monitored the effects of TM-dipyridamole on the transport of the vesicular stomatitis virus glycoprotein (VSVG) in a pulse-chase experiment. VSVG trafficking from the ER to the Golgi is monitored by the conversion of N-linked sugars from an endoglycosidase H (endoH)-sensitive form (ER) to an endoH-resistant form (Golgi). Whereas the non-selective inhibitor brefeldin A prevented conversion to the endoH-resistant form, treatment with TM-dipyridamole did not prevent this transition, confirming that TM-dipyridamole does not inhibit general ER-to-Golgi protein trafficking and is therefore selective for SCAP-SREBP transport (Figure 5F).

A "Clickable" Photoaffinity Dipyridamole Derivative, PF-07079672, Binds to INSIG and SCAP

The studies presented so far demonstrate that dipyridamole and TM-dipyridamole block SREBP maturation by inhibiting ER-to-Golgi trafficking, and that manipulation of SCAP or INSIG levels

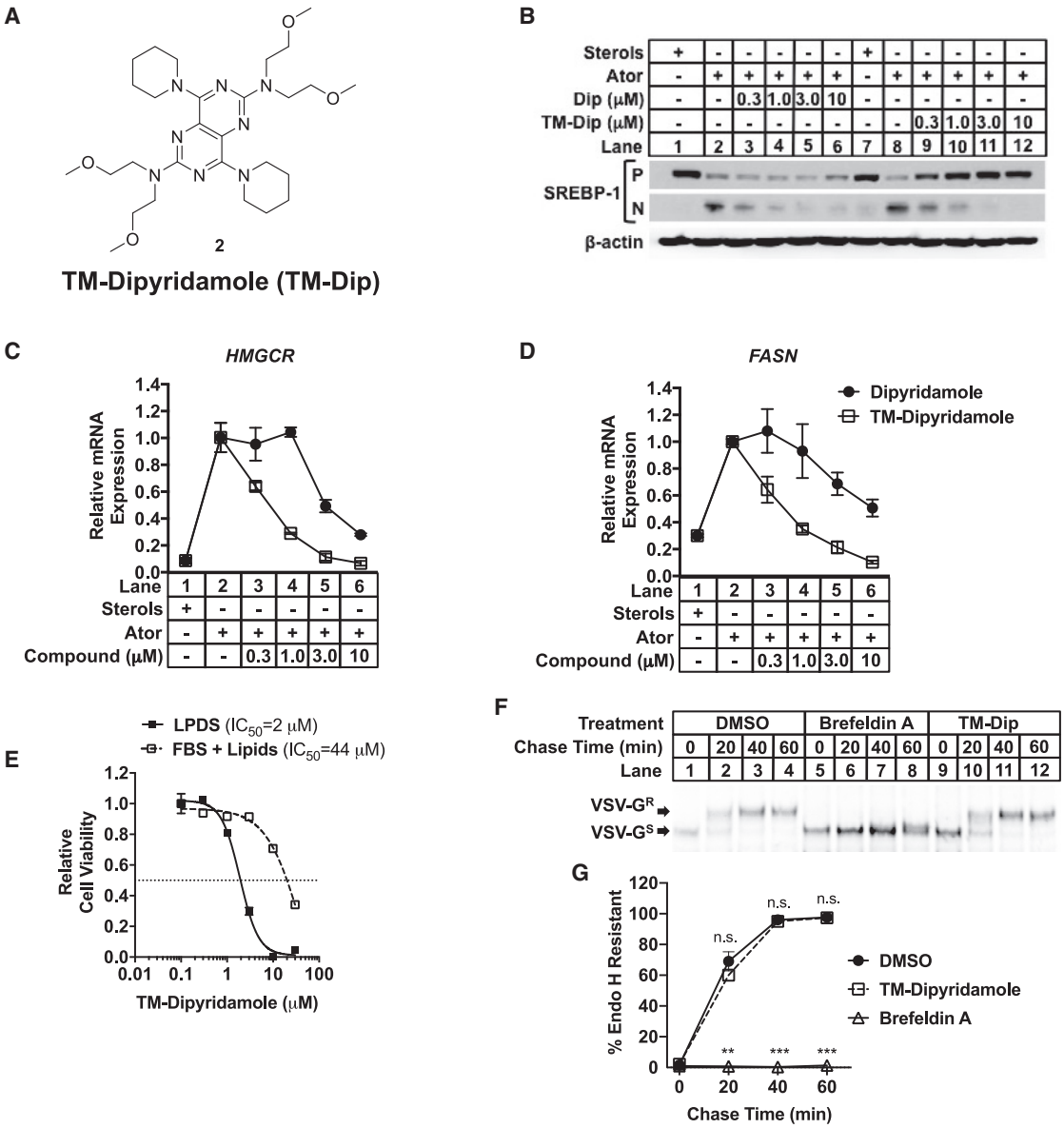

Figure 5. N2,N2,N6,N6-tetrakis(2-methoxyethyl)-4,8-di(piperidin-1-yl)pyrimido[5,4-d]pyrimidine-2,6-diamine Blocks SREBP Maturation

(A) Structure of a modified dipyridamole derivative (N2,N2,N6,N6-tetrakis(2-methoxyethyl)-4,8-di(piperidin-1-yl)pyrimido[5,4-d]pyrimidine-2,6-diamine [TM-dipyridamole]).

(B–D) HeLa cells were incubated in DMEM containing 5% LPDS with sterols (12 μg/mL cholesterol and 1 μg/mL 25-OH cholesterol) or atorvastatin (Ator) (10 μM) with increasing concentrations of dipyridamole (Dip) or TM-dipyridamole (TM-Dip). After 16 h incubation, cells were harvested and RNA and protein extracts were prepared. (B) Immunoblots for precursor (P) and nuclear (N) SREBP-1 and β-actin. (C and D) *HMGCR* and *FASN* mRNA expression was measured using qPCR. Gene expression data were from three biological replicates (mean ± SEM).

(E) Wild-type CHO-7 cells were seeded at a density of 5,000 cells per well (96-well plate) in DMEM/F-12 (1:1) medium (containing 100 units/mL penicillin and 100 μg/mL streptomycin sulfate) supplemented with 5% (v/v) LPDS or 5% (v/v) fetal bovine serum (FBS), 5 μg/mL cholesterol, 1 mM sodium mevalonate, and 20 μM sodium oleate containing the indicated concentration of TM-dipyridamole. Seventy-two hours later, MTS (15 μL per well) was added, and cells were incubated at 37°C for 3 h, and A_{490} was measured. Viability was normalized to vehicle-treated conditions. Error bars represent the SEM from four technical replicates (mean ± SEM).

(F) CHO-7 cells were infected with vesicular stomatitis virus and, after 3.5 h, cells were pre-treated, starved, labeled with ^{35}S-Met, and then chased for the indicated times in the presence of vehicle (0.1% DMSO), brefeldin A (5 μg/mL), or TM-dipyridamole (3 μM). Cell lysates were treated directly with endoH, resolved 4%–12% NU-PAGE, and dried gels were imaged on a molecular Imager FX PhosphorImager.

(G) Data are the average of three biological replicates. Error bars represent ± SEM. Student's t test was used to evaluate statistical significance comparing treatment and vehicle, **p < 0.01, ***p < 0.001; n.s., not significant.

See also Figure S4.

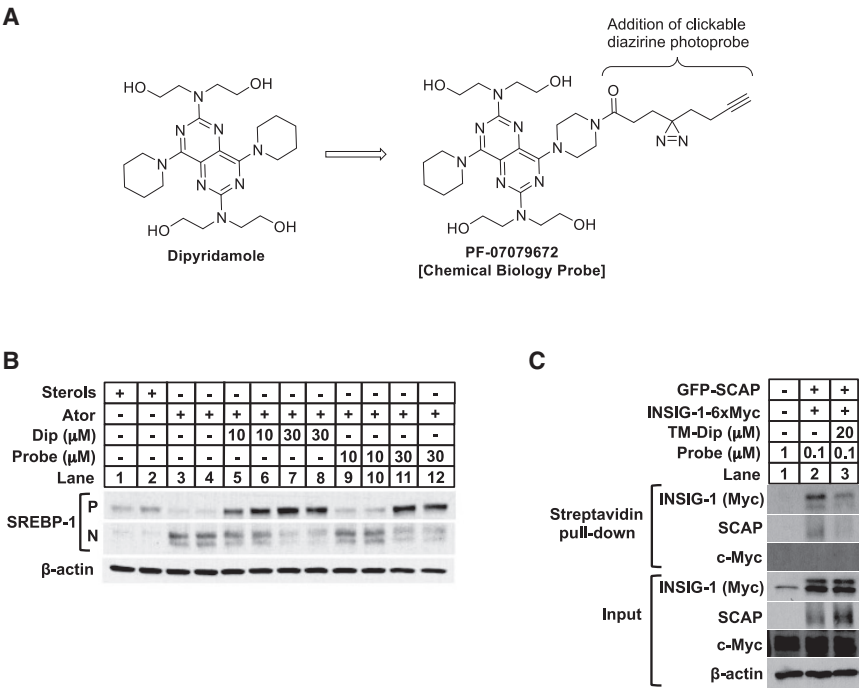

Figure 6. Photo-reactive Dipyridamole Probe Binds to INSIG and SCAP

(A) Structure of the clickable photoaffinity dipyridamole derivative PF-07079672.

(B) HepG2 cells incubated in DMEM with 5% LPDS containing sterols (12 μg/mL cholesterol and 1 μg/mL 25-OH cholesterol) or atorvastatin (Ator) (10 μM) with either dipyridamole (Dip) (10 and 30 μM) or PF-07079672 "probe" (10 and 30 μM) as indicated. After 16 h incubation, cell extracts were used for immunoblotting for endogenous SREBP-1 or β-actin.

(C) HEK293T cells were co-transfected with pCMV-GFP-SCAP and pCMV-INSIG-1-6X-Myc and incubated in DMEM medium with atorvastatin overnight. Cells were treated with PF-07079672 photoprobe (0.1 μM) ± TM-dipyridamole (20 μM) for 1 h each before UV crosslinking, cell lysis, and click chemistry as described in the STAR Methods. Probe-labeled proteins were enriched on streptavidin matrix. Input and bound protein fractions were then immunoblotted for endogenous c-Myc, Myc-tagged INSIG, SCAP (IgG-9D5), or β-actin as indicated.

altered the sensitivity to inhibition. These data suggest that the inhibitors may directly interact with SCAP or INSIG. To evaluate this, we synthesized a dipyridamole derivative that contains a photoactivatable diazirine and a "clickable" alkyne handle (Figure 6A). The photosensitive-analog inhibited SREBP maturation similar to the parental dipyridamole (Figure 6B). We then expressed GFP-SCAP and/or Myc-INSIG-1 in HEK293T cells and co-treated the cells with the photo-clickable probe incubated in the absence or presence of an excess of TM-dipyridamole. After UV irradiation, cell lysis, and click chemistry with biotin-azide, we performed a pull-down assay with streptavidin beads after activating the photoprobe and followed the results through immunoblotting. We found that the photo-clickable probe was able to pull down both GFP-tagged SCAP and Myc-tagged INSIG-1, which was blocked when we included 200× excess of TM-dipyridamole (Figure 6C). In contrast, endogenous c-Myc was not enriched by streptavidin pull-down. Collectively, these results indicate that dipyridamole and its analogs bind directly to either SCAP, INSIG, or both.

DISCUSSION

SREBPs control flux of acetyl-CoA into both the fatty acid and mevalonate synthetic pathways providing key lipid building blocks required for cell membranes. SREBPs are selectively increased in several cancer models to increase *de novo* lipid synthesis required to satisfy their increased demand for both cholesterol and fatty acids (Mullen et al., 2016). Thus, selectively targeting SREBPs would simultaneously limit flux into synthesis of both lipid classes and would be more effective than compounds that target either pathway separately.

Because SCAP is essential for activating both SREBP-1 and SREBP-2, and has no other known biological function (Brown et al., 2018), it is an attractive therapeutic target that would affect both pathways. In this article, we have identified dipyridamole as a candidate inhibitor of SCAP-dependent SREBP maturation. Dipyridamole was first reported by Pandyra et al. (2014) to increase the modest growth inhibitory effect of statins in a leukemia mouse model and they further showed that it might act by limiting the accumulation of nuclear SREBPs (Pandyra et al., 2014). Dipyridamole is a pyrimidine analog and known PDE inhibitor approved by the FDA for treatment of blood-clotting disorders, and at higher doses is effective as a short-term vasodilator (Kerndt and Nagalli, 2020). However, the mechanism for how dipyridamole inhibits SREBP maturation and lipid synthesis and whether this was dependent on the PDE inhibitory action of dipyridamole was unclear.

We found that addition of dipyridamole to cultured cells resulted in retention of the precursor SREBP in the ER and the effect was sufficient to override the normal cellular response to both low sterol levels and insulin signaling *in vivo*, two metabolic situations where the SCAP-SREBP complex normally traffics from the ER to the Golgi apparatus. Mechanistically, dipyridamole increased the stability of ER-localized INSIG-1 protein in cultured cells (Figures 4A and 4B) and Insig-2 protein in mouse liver (Figure 4C). We showed that when cells were treated with a clickable photoprobe derivative of dipyridamole that both SCAP and INSIG were selectively pulled down, consistent with a direct role for dipyridamole in SCAP/SREBP function.

Similar to other ER membrane-resident proteins, INSIGs are degraded through the ER-associated degradation pathway (ERAD). Three distinct ER resident E3 ubiquitin ligases have been implicated (Jiang et al., 2018; Jo et al., 2011; Liu et al., 2012) along with associated proteins that help deliver the ubiquitinated INSIGs to the proteasome (Lee et al., 2008). Whether dipyridamole increases INSIG levels by simply promoting the

interaction between INSIG and SCAP similar to oxysterols (Gong et al., 2006; Radhakrishnan et al., 2007), or whether dipyridamole might directly target a post-ubiquitination step in the ERAD-dependent degradation of INSIGs similar to what has been proposed for unsaturated fatty acids (Lee et al., 2008), is an area that warrants further investigation.

Dipyridamole has intrinsic PDE inhibitory activity. We succeeded in modifying dipyridamole to remove these PDE inhibitory properties while increasing the potency of inhibiting SREBP. When the four free hydroxyl groups of dipyridamole were changed to -CH_3O, the resulting modified dipyridamole derivative (TM-dipyridamole) was even more potent at limiting SREBP activation. Even though TM-dipyridamole retained SREBP inhibition, this derivatization significantly blunted the PDE inhibitory activity that is intrinsic to dipyridamole. This suggests that the effects of dipyridamole on SREBP are not through PDE inhibition. The effects of dipyridamole are also independent of cAMP- and cGMP-dependent signaling pathways (Figure S3). In addition, we showed that dipyridamole did not prevent the ER-to-Golgi movement of the VSVG protein, confirming that it does not have a broad and non-selective role in inhibiting general COPII-dependent trafficking.

Two other small molecules have been reported to limit ER-to-Golgi trafficking of SCAP-SREBP. Fatostatin was originally identified as a molecule that limited lipid storage in cultured adipocytes (Choi et al., 2003) and was subsequently shown to bind SCAP and limit nuclear accumulation of SREBP (Kamisuki et al., 2009). Betulin is derived from the bark of the birch tree, and it limits migration of SCAP-SREBP to the Golgi (Tang et al., 2011). Horton and colleagues (Moon et al., 2012) demonstrated that genetic deletion of SCAP limited hepatic steatosis but failed to reduce body weight in *ob/ob* mice. In contrast, both fatostatin and betulin treatment in mice resulted in reduced body weight in addition to reduced liver fat accumulation. Thus, these two compounds likely have additional effects in addition to limiting SREBP maturation. In fact, fatostatin inhibited movement of VSVG from the ER-to-Golgi so it is not selective for SCAP-SREBP (Shao et al., 2016). The specificity of betulin has not been established, but we showed that it did not limit CHO-7 growth in sterol-depleted culture medium at concentrations used in the original paper (data not shown). In addition, betulin inhibits mammalian target of rapamycin activity (Lin et al., 2020), which as mentioned below also stimulates SREBP maturation. Thus, it is also unlikely that betulin is a selective inhibitor of the SCAP-SREBP pathway. In contrast, our studies have identified a selective and effective SREBP inhibitor that is an attractive candidate for further structural refinement.

Significance

We uncovered the mechanism by which dipyridamole inhibits SREBP processing by directly binding to SCAP and INSIG limiting SCAP-SREBP complex movement from ER to the Golgi apparatus. Statins have potential as anti-tumor agents because of their effects on suppressing the mevalonate pathway (Mullen et al., 2016) and this can be augmented by SREBP inhibition. Thus, a two-pronged approach using statins and compounds that decrease nuclear SREBP represents a potential therapeutic targeting strategy for cancers that rely on lipids and the mevalonate pathway for tumorigenicity. Unfortunately, chronic treatment with phosphodiesterase inhibitors can result in significant weight loss through increased adipose tissue lipolysis and we confirmed this effect for dipyridamole in mice (data not shown). We successfully separated the effects of dipyridamole on PDE and SREBP through a simple modification of the dipyridamole structure; however, TM-dipyridamole is very hydrophobic and in preliminary pharmacological studies in mice it was not highly bioavailable. Nonetheless, these observations provide a starting point for a focused structure-function analysis using dipyridamole or TM-dipyridamole as a starting compound for novel and selective inhibitors of the SREBP pathway.

STAR★METHODS

Detailed methods are provided in the online version of this paper and include the following:

- KEY RESOURCES TABLE
- RESOURCE AVAILABILITY
  - Lead Contact
  - Materials Availability
  - Data and Code Availability
- EXPERIMENTAL MODEL AND SUBJECT DETAILS
  - Animal Experiments
  - Cell Culture
- METHOD DETAILS
  - Nuclear Fractionation
  - Membrane Fractionation
  - Modification of Dipyridamole
  - Lipid Dependent Growth Assay
  - VSVG Maturation Assay
  - Transfection
  - Co-immunoprecipitation
  - Immunoblotting
  - Immunostaining
  - PDE5A Phosphodiesterase Inhibitor Assay
  - Click Chemistry
  - RNA Isolation and Gene Expression Analysis
- QUANTIFICATION AND STATISTICAL ANALYSIS

SUPPLEMENTAL INFORMATION

Supplemental Information can be found online at https://doi.org/10.1016/j.chembiol.2020.10.003.

ACKNOWLEDGMENTS

We are grateful to Dr. Linda Penn for introducing us to the dipyridamole project. We thank Drs. Michael S. Brown and Joseph L. Goldstein for providing us CHO-7 cells; Dr. Jared Rutter for pQCXIN-3xFLAG-SREBP plasmids; Dr. Fabienne Foufelle for the Insig2 antibody; Dr. Russell DeBose-Boyd for the Myc-S1P-KDEL plasmid; and Pfizer Inc for the clickable photoprobe PF-07079672. We are also grateful to our former student interns Rupert Faltlhauser and Mitchell Thomas for their dedication and technical assistance. We thank the Sanford Burnham Prebys Medical Discovery Institute Cell Imaging Core (Humberto Ibarra Avila). This research was supported by NIH, United States grants HL48044 (to T.F.O.) and HL077588 (to P.J.E.).

AUTHOR CONTRIBUTIONS

Conceptualization, R.M.E. and T.F.O.; Methodology, R.M.E., M.R.-R., W.S., P.E.P., U.S., C.W.a.E., P.M.H., C.E.M., P.J.E., and T.F.O.; Investigation, R.M.E., M.R.-R., W.S., P.E.P., and U.S.; Resources, C.W.a.E., P.M.H., C.E.M., P.J.E., and T.F.O.; Writing – Original Draft, R.M.E. and T.F.O.; Writing – Review & Editing, R.M.E., M.R.-R., W.S., P.E.P., C.W.a.E., P.M.H., C.E.M., P.J.E., and T.F.O.; Supervision, R.M.E., P.J.E., and T.F.O.; Project Administration, R.M.E. and T.F.O.; Funding Acquisition, P.J.E. and T.F.O.

DECLARATION OF INTERESTS

During completion of these studies, R.M.E., U.S., and C.W.a.E. were employed by Pfizer Inc. and M.R.-R. was employed by Enanta Pharmaceuticals.

Received: August 13, 2020
Revised: September 10, 2020
Accepted: October 5, 2020
Published: October 22, 2020

REFERENCES

Adams, C.M., Reitz, J., De Brabander, J.K., Feramisco, J.D., Li, L., Brown, M.S., and Goldstein, J.L. (2004). Cholesterol and 25-hydroxycholesterol inhibit activation of SREBPs by different mechanisms, both involving SCAP and Insigs. J. Biol. Chem. *279*, 52772–52780.

Brown, M.S., Radhakrishnan, A., and Goldstein, J.L. (2018). Retrospective on cholesterol homeostasis: the central role of Scap. Annu. Rev. Biochem. *87*, 783–807.

Choi, Y., Kawazoe, Y., Murakami, K., Misawa, H., and Uesugi, M. (2003). Identification of bioactive molecules by adipogenesis profiling of organic compounds. J. Biol. Chem. *278*, 7320–7324.

Cluett, E.B., Kuismanen, E., and Machamer, C.E. (1997). Heterogeneous distribution of the unusual phospholipid semilysobisphosphatidic acid through the Golgi complex. Mol. Biol. Cell *8*, 2233–2240.

Curtin, N.J., Barlow, H.C., Bowman, K.J., Calvert, A.H., Davison, R., Golding, B.T., Huang, B., Loughlin, P.J., Newell, D.R., Smith, P.G., et al. (2004). Resistance-modifying agents. 11. (1) Pyrimido[5,4-d]pyrimidine modulators of antitumor drug activity. Synthesis and structure-activity relationships for nucleoside transport inhibition and binding to alpha1-acid glycoprotein. J. Med. Chem. *47*, 4905–4922.

DeBose-Boyd, R.A., Brown, M.S., Li, W.P., Nohturfft, A., Goldstein, J.L., and Espenshade, P.J. (1999). Transport-dependent proteolysis of SREBP: relocation of site-1 protease from Golgi to ER obviates the need for SREBP transport to Golgi. Cell *99*, 703–712.

Engelking, L.J., Kuriyama, H., Hammer, R.E., Horton, J.D., Brown, M.S., Goldstein, J.L., and Liang, G. (2004). Overexpression of Insig-1 in the livers of transgenic mice inhibits SREBP processing and reduces insulin-stimulated lipogenesis. J. Clin. Invest. *113*, 1168–1175.

Gong, Y., Lee, J.N., Lee, P.C., Goldstein, J.L., Brown, M.S., and Ye, J. (2006). Sterol-regulated ubiquitination and degradation of Insig-1 creates a convergent mechanism for feedback control of cholesterol synthesis and uptake. Cell Metab. *3*, 15–24.

Hegarty, B.D., Bobard, A., Hainault, I., Ferré, P., Bossard, P., and Foufelle, F. (2005). Distinct roles of insulin and liver X receptor in the induction and cleavage of sterol regulatory element-binding protein-1c. Proc. Natl. Acad. Sci. U S A *102*, 791–796.

Horton, J.D., Bashmakov, Y., Shimomura, I., and Shimano, H. (1998). Regulation of sterol regulatory element binding proteins in livers of fasted and refed mice. Proc. Natl. Acad. Sci. U S A *95*, 5987–5992.

Horton, J.D., Goldstein, J.L., and Brown, M.S. (2002). SREBPs: activators of the complete program of cholesterol and fatty acid synthesis in the liver. J. Clin. Invest. *109*, 1125–1131.

Hua, X., Nohturfft, A., Goldstein, J.L., and Brown, M.S. (1996). Sterol resistance in CHO cells traced to point mutation in SREBP cleavage-activating protein. Cell *87*, 415–426.

Hua, X., Yokoyama, C., Wu, J., Briggs, M.R., Brown, M.S., Goldstein, J.L., and Wang, X. (1993). SREBP-2, a second basic-helix-loop-helix-leucine zipper protein that stimulates transcription by binding to a sterol regulatory element. Proc. Natl. Acad. Sci. U S A *90*, 11603–11607.

Huang, Z., Ogasawara, D., Seneviratne, U.I., Cognetta, A.B., 3rd, Am Ende, C.W., Nason, D.M., Lapham, K., Litchfield, J., Johnson, D.S., and Cravatt, B.F. (2019). Global portrait of protein targets of metabolites of the neurotoxic compound BIA 10-2474. ACS Chem. Biol. *14*, 192–197.

Jiang, L.Y., Jiang, W., Tian, N., Xiong, Y.N., Liu, J., Wei, J., Wu, K.Y., Luo, J., Shi, X.J., and Song, B.L. (2018). Ring finger protein 145 (RNF145) is a ubiquitin ligase for sterol-induced degradation of HMG-CoA reductase. J. Biol. Chem. *293*, 4047–4055.

Jo, Y., Lee, P.C., Sguigna, P.V., and DeBose-Boyd, R.A. (2011). Sterol-induced degradation of HMG CoA reductase depends on interplay of two Insigs and two ubiquitin ligases, gp78 and Trc8. Proc. Natl. Acad. Sci. U S A *108*, 20503–20508.

Kamisuki, S., Mao, Q., Abu-Elheiga, L., Gu, Z., Kugimiya, A., Kwon, Y., Shinohara, T., Kawazoe, Y., Sato, S., Asakura, K., et al. (2009). A small molecule that blocks fat synthesis by inhibiting the activation of SREBP. Chem. Biol. *16*, 882–892.

Kerndt, C., and Nagalli, S. (2020). Dipyridamole. StatPearls (Treasure Island (FL): StatPearls Publishing (StatPearls Publishing LLC).

Kim, H.H., and Liao, J.K. (2008). Translational therapeutics of dipyridamole. Arterioscler Thromb. Vasc. Biol. *28*, 39–42.

Lee, J.N., Zhang, X., Feramisco, J.D., Gong, Y., and Ye, J. (2008). Unsaturated fatty acids inhibit proteasomal degradation of Insig-1 at a postubiquitination step. J. Biol. Chem. *283*, 33772–33783.

Lin, W., and Buolamwini, J.K. (2007). Synthesis, flow cytometric evaluation, and identification of highly potent dipyridamole analogues as equilibrative nucleoside transporter 1 inhibitors. J. Med. Chem. *50*, 3906–3920.

Lin, Y.C., Chen, H.Y., Hsieh, C.P., Huang, Y.F., and Chang, I.L. (2020). Betulin inhibits mTOR and induces autophagy to promote apoptosis in human osteosarcoma cell lines. Environ. Toxicol. *35*, 879–887.

Liu, T.F., Tang, J.J., Li, P.S., Shen, Y., Li, J.G., Miao, H.H., Li, B.L., and Song, B.L. (2012). Ablation of gp78 in liver improves hyperlipidemia and insulin resistance by inhibiting SREBP to decrease lipid biosynthesis. Cell Metab. *16*, 213–225.

Longo, J., Mullen, P.J., Yu, R., van Leeuwen, J.E., Masoomian, M., Woon, D.T.S., Wang, Y., Chen, E.X., Hamilton, R.J., Sweet, J.M., et al. (2019). An actionable sterol-regulated feedback loop modulates statin sensitivity in prostate cancer. Mol. Metab. *25*, 119–130.

Metherall, J.E., Goldstein, J.L., Luskey, K.L., and Brown, M.S. (1989). Loss of transcriptional repression of three sterol-regulated genes in mutant hamster cells. J. Biol. Chem. *264*, 15634–15641.

Moon, Y.A., Liang, G., Xie, X., Frank-Kamenetsky, M., Fitzgerald, K., Koteliansky, V., Brown, M.S., Goldstein, J.L., and Horton, J.D. (2012). The Scap/SREBP pathway is essential for developing diabetic fatty liver and carbohydrate-induced hypertriglyceridemia in animals. Cell Metab. *15*, 240–246.

Mullen, P.J., Yu, R., Longo, J., Archer, M.C., and Penn, L.Z. (2016). The interplay between cell signalling and the mevalonate pathway in cancer. Nat. Rev. Cancer *16*, 718–731.

Nohturfft, A., Yabe, D., Goldstein, J.L., Brown, M.S., and Espenshade, P.J. (2000). Regulated step in cholesterol feedback localized to budding of SCAP from ER membranes. Cell *102*, 315–323.

Pandyra, A., Mullen, P.J., Kalkat, M., Yu, R., Pong, J.T., Li, Z., Trudel, S., Lang, K.S., Minden, M.D., Schimmer, A.D., et al. (2014). Immediate utility of two approved agents to target both the metabolic mevalonate pathway and its restorative feedback loop. Cancer Res. *74*, 4772–4782.

Radhakrishnan, A., Ikeda, Y., Kwon, H.J., Brown, M.S., and Goldstein, J.L. (2007). Sterol-regulated transport of SREBPs from endoplasmic reticulum to Golgi: oxysterols block transport by binding to Insig. Proc. Natl. Acad. Sci. U S A *104*, 6511–6518.

Radhakrishnan, A., Sun, L.P., Kwon, H.J., Brown, M.S., and Goldstein, J.L. (2004). Direct binding of cholesterol to the purified membrane region of SCAP: mechanism for a sterol-sensing domain. Mol. Cell *15*, 259–268.

Rawson, R.B., Zelenski, N.G., Nijhawan, D., Ye, J., Sakai, J., Hasan, M.T., Chang, T.Y., Brown, M.S., and Goldstein, J.L. (1997). Complementation cloning of S2P, a gene encoding a putative metalloprotease required for intramembrane cleavage of SREBPs. Mol. Cell *1*, 47–57.

Roqueta-Rivera, M., Esquejo, R.M., Phelan, P.E., Sandor, K., Daniel, B., Foufelle, F., Ding, J., Li, X., Khorasanizadeh, S., and Osborne, T.F. (2016). SETDB2 links glucocorticoid to lipid metabolism through Insig2a regulation. Cell Metab. *24*, 474–484.

Sakai, J., Duncan, E.A., Rawson, R.B., Hua, X., Brown, M.S., and Goldstein, J.L. (1996). Sterol-regulated release of SREBP-2 from cell membranes requires two sequential cleavages, one within a transmembrane segment. Cell *85*, 1037–1046.

Sakai, J., Nohturfft, A., Cheng, D., Ho, Y.K., Brown, M.S., and Goldstein, J.L. (1997). Identification of complexes between the COOH-terminal domains of sterol regulatory element-binding proteins (SREBPs) and SREBP cleavage-activating protein. J. Biol. Chem. *272*, 20213–20221.

Seo, Y.K., Jeon, T.I., Chong, H.K., Biesinger, J., Xie, X., and Osborne, T.F. (2011). Genome-wide localization of SREBP-2 in hepatic chromatin predicts a role in autophagy. Cell Metab. *13*, 367–375.

Shao, W., Machamer, C.E., and Espenshade, P.J. (2016). Fatostatin blocks ER exit of SCAP but inhibits cell growth in a SCAP-independent manner. J. Lipid Res. *57*, 1564–1573.

Shimomura, I., Shimano, H., Horton, J.D., Goldstein, J.L., and Brown, M.S. (1997). Differential expression of exons 1a and 1c in mRNAs for sterol regulatory element binding protein-1 in human and mouse organs and cultured cells. J. Clin. Invest. *99*, 838–845.

Shimomura, I., Bashmokav, Y., and Horton, J.D. (1999). Increased levels of nuclear SREBP-1c associated with fatty livers in two mouse models of diabetes mellitus. J. Biol. Chem. *274*, 30028–30032.

Tang, J.J., Li, J.G., Qi, W., Qiu, W.W., Li, P.S., Li, B.L., and Song, B.L. (2011). Inhibition of SREBP by a small molecule, betulin, improves hyperlipidemia and insulin resistance and reduces atherosclerotic plaques. Cell Metab. *13*, 44–56.

Toth, J.I., Datta, S., Athanikar, J.N., Freedman, L.P., and Osborne, T.F. (2004). Selective coactivator interactions in gene activation by SREBP-1a and -1c. Mol. Cell Biol. *24*, 8288–8300.

Wu, X., Romero, D., Swiatek, W.I., Dorweiler, I., Kikani, C.K., Sabic, H., Zweifel, B.S., McKearn, J., Blitzer, J.T., Nickols, G.A., et al. (2014). PAS kinase drives lipogenesis through SREBP-1 maturation. Cell Rep. *8*, 242–255.

Xu, H., Jesson, M.I., Seneviratne, U.I., Lin, T.H., Sharif, M.N., Xue, L., Nguyen, C., Everley, R.A., Trujillo, J.I., Johnson, D.S., et al. (2019). PF-06651600, a dual JAK3/TEC family kinase inhibitor. ACS Chem. Biol. *14*, 1235–1242.

Yabe, D., Xia, Z.P., Adams, C.M., and Rawson, R.B. (2002). Three mutations in sterol-sensing domain of SCAP block interaction with insig and render SREBP cleavage insensitive to sterols. Proc. Natl. Acad. Sci. U S A *99*, 16672–16677.

Yang, T., Espenshade, P.J., Wright, M.E., Yabe, D., Gong, Y., Aebersold, R., Goldstein, J.L., and Brown, M.S. (2002). Crucial step in cholesterol homeostasis: sterols promote binding of SCAP to INSIG-1, a membrane protein that facilitates retention of SREBPs in ER. Cell *110*, 489–500.

Yokoyama, C., Wang, X., Briggs, M.R., Admon, A., Wu, J., Hua, X., Goldstein, J.L., and Brown, M.S. (1993). SREBP-1, a basic-helix-loop-helix-zipper protein that controls transcription of the low density receptor gene. Cell *75*, 185–197.

STAR★METHODS

KEY RESOURCES TABLE

REAGENT or RESOURCE	SOURCE	IDENTIFIER
Antibodies		
Rabbit polyclonal anti-Calnexin	Abcam	Cat#ab22595; RRID:AB_2069006
Mouse monoclonal anti-SREBP-1	ATCC	Cat#CRL-2121; RRID:AB_2255229
Rabbit monoclonal anti-AKT	Cell Signaling Technology	Cat#4685; RRID:AB_2225340
Rabbit monoclonal anti-phospho-AKT (Ser473)	Cell Signaling Technology	Cat#4060; RRID:AB_2315049
Rabbit monoclonal anti-phospho-AKT (Thr308)	Cell Signaling Technology	Cat#13038; RRID:AB_2629447
Rabbit monoclonal anti-phospho-PKA substrate (RRXS*/T*)	Cell Signaling Technology	Cat#9624; RRID:AB_331817
Rabbit monoclonal anti-RCAS1	Cell Signaling Technology	Cat#12290; RRID:AB_2736985
Rabbit monoclonal anti-S6	Cell Signaling Technology	Cat#2217; RRID:AB_331355
Rabbit monoclonal anti-phospho-S6 Ribosomal Protein (Ser240/244)	Cell Signaling Technology	Cat#5364; RRID:AB_10694233
Anti-mouse IgG, HRP-linked antibody	Cell Signaling Technology	Cat#7076; RRID:AB_330924
Anti-rabbit IgG, HRP-linked antibody	Cell Signaling Technology	Cat#7074; RRID:AB_2099233
Mouse monoclonal anti-Myc	Santa Cruz Biotechnology	Cat#sc-40; RRID:AB_627268
Mouse monoclonal anti-SCAP	Santa Cruz Biotechnology	Cat#sc-13553; RRID:AB_628237
Mouse monoclonal anti-YY-1	Santa Cruz Biotechnology	Cat#sc-7341; RRID:AB_2257497
Mouse monoclonal anti-beta actin	Sigma-Aldrich	Cat#A2228; RRID:AB_476697
Mouse monoclonal anti-FLAG M2	Sigma-Aldrich	Cat#F1804; RRID:AB_262044
Goat anti-Rabbit IgG (H+L) Cross-Adsorbed Secondary Antibody, Alexa Fluor 488	Thermo Fisher	Cat#A-11008; RRID:AB_143165
Goat anti-Rabbit IgG (H+L) Cross-Adsorbed Secondary Antibody, Cy5	Thermo Fisher	Cat#A10523; RRID:AB_2534032
Rabbit polyclonal anti-SREBP-2	Seo et al., 2011 PMID: 21459322	N/A
Rabbit polyclonal anti-Insig2	Hegarty et al., 2005 PMID: 15637161	N/A
Chemicals, Peptides, and Recombinant Proteins		
Lipoprotein deficient serum, bovine	Alfa Aesar	Cat#J65182
iScript™ cDNA Synthesis Kit	Bio-Rad	Cat#1708891
SsoFast EvaGreen Supermix	Bio-Rad	Cat# 1725202
4x Laemmli Sample Buffer	Bio-Rad	Cat#1610747
Brefeldin A	Cayman Chemical	Cat#11861-5
Atorvastatin, calcium salt	Cayman Chemical	Cat#10493
Cycloheximide	Cayman Chemical	Cat#14126
Forskolin	Cayman Chemical	Cat#11018
Methanol	Fisher Scientific	Cat#A456-4
Chloroform	Fisher Scientific	Cat#C297-4
Zymo Research Direct-zol RNA MiniPrep kit	Genesee Scientific	Cat#11-331
Sodium dodecyl sulfate (SDS)	Invitrogen	Cat#15553035
Dulbecco's Phosphate-buffered saline (DPBS)	Life Technologies	Cat#14190144
Distilled Water	Life Technologies	Cat#15230-162

(*Continued on next page*)

Continued

REAGENT or RESOURCE	SOURCE	IDENTIFIER
Persantine (dipyridamole) (*in vivo*)	McKesson Medical Prescription Drugs	Cat#455343
Endoglycosidase H	New England BioLabs	Cat#P0702
[^{35}S] EasyTag Express Protein Mix	Perkin Elmer	Cat#NEG77200
PF-07079672 (clickable photoprobe)	Pfizer Inc.	N/A
8-pCPT-cGMP	Sigma-Aldrich	Cat#C5438
Lipoprotein deficient serum from fetal calf	Sigma-Aldrich	Cat#S5394
Hydroxypropyl-β-cyclodextrin	Sigma-Aldrich	Cat#H5784
tert-butanol (t-BuOH)	Sigma-Aldrich	Cat#19640
Copper(II) sulfate (CuSO4)	Sigma-Aldrich	Cat#C1297
PEG-600	Sigma-Aldrich	Cat#202401
DL-Tartaric acid	Sigma-Aldrich	Cat#T400
Protease inhibitor cocktail	Sigma-Aldrich	Cat#P3840
5-Cholesterol (5-Cholesten-3 beta-OL)	Steraloids Inc.	Cat#C6760-000
25-hydroxycholesterol (5-Cholesten-3 beta, 25-Diol)	Steraloids Inc.	Cat#C6510-000
Tris(benzyltriazolylmethyl)amine (TBTA)	TCI	Cat#T2993
IBMX	Tocris Bioscience	Cat#2845
Dipyridamole (*in vitro*)	Tocris Bioscience	Cat#0691
ProLong Gold Antifade Mountant	Thermo Fisher Scientific	Cat#P36930
Dynabeads Protein G for Immunoprecipitation	Thermo Fisher Scientific	Cat#10003D
Lipofectamine™ 2000 Transfection Reagent	Thermo Fisher Scientific	Cat#11668019
SuperSignal™ West Pico Chemiluminescent Substrate	Thermo Fisher Scientific	Cat#PI34080
Tris(2-carboxyethyl)phosphine HCl (TCEP)	Thermo Fisher Scientific	Cat#20491
High capacity Streptavidin agarose resin	Thermo Fisher Scientific	Cat#20359
Phenylmethylsulfonyl fluoride	Thermo Fisher Scientific	Cat#36978
Halt's phosphatase inhibitor	Thermo Fisher Scientific	Cat#78440
TM-dipyridamole	This paper	N/A
Tetramethylrhodamine (TAMRA)-biotin-azide	Huang et al., 2019 PMID: 30702848	N/A
VSV (San Juan strain, Indiana serotype)	Cluett et al., 1997 PMID: 9362065	N/A
Critical Commercial Assays		
CellTiter 96 Aqueous one solution Cell Proliferation Assay (MTS)	Promega	Cat#G3580
PDE5A1 Assay Kit	BPS Bioscience	Cat#60351
Pierce™ BCA Protein Assay Kit	Thermo Fisher	Cat#PI23223
Experimental Models: Cell Lines		
Human: HeLa	ATCC	Cat# CCL-2, RRID:CVCL_0030
Human: HEK293T	ATCC	Cat# CRL-11268, RRID:CVCL_1926
Human: HepG2	ATCC	Cat# HB-8065, RRID:CVCL_0027
Hamster: CHO-7	Metherall et al., 1989 PMID: 2570073	N/A
Hamster: CHO/pGFP-SCAP	Nohturfft et al., 2000 PMID: 10975522	N/A
Experimental Models: Organisms/Strains		
Mouse: C57BL/6J	The Jackson Laboratory	JAX: 000664

(*Continued on next page*)

Continued

REAGENT or RESOURCE	SOURCE	IDENTIFIER
Oligonucleotides		
siRNA against human INSIG1 (SMARTPool: ON-Target Plus)	GE Healthcare	Cat#L-017880-00-0005
siRNA against human INSIG2 (SMARTPool: ON-Target Plus)	GE Healthcare	Cat#L-021039-00-0005
siRNA Non-Targeting Control (ON-TARGETplus Non-targeting Pool)	GE Healthcare	Cat#D-001810-10-05
Primers for qPCR, see Table S1	This paper	N/A
Recombinant DNA		
Plasmid: pCMV-Insig-1-6xMyc	ATCC	Cat#88099
Plasmid: pQCXIN-3xFLAG-pSREBP-1a	Wu et al., 2014 PMID: 25001282	N/A
Plasmid: pQCXIN-3xFLAG-pSREBP-1c	Wu et al., 2014 PMID: 25001282	N/A
Plasmid: pQCXIN-3xFLAG-pSREBP-2	Laboratory of Dr. Jared Rutter	N/A
Plasmid: pcDNA3.1-2xFLAG-nSREBP-2	Toth et al., 2004 PMID: 15340088	Addgene Plasmid #26807
Plasmid: pcDNA3.0-GFP-SCAP	Nohturfft et al., 2000 PMID: 10975522	N/A
Plasmid: pCMV-S1P-Myc-KDEL	DeBose-Boyd et al., 1999 PMID: 10619424	N/A
Software and Algorithms		
ImageQuant TL	GE Healthcare Life Sciences	www.gelifesciences.com/
GraphPad Prism 8	GraphPad	www.graphpad.com/scientific-software/prism/
Volocity	Perkin-Elmer	www.perkinelmer.com/

RESOURCE AVAILABILITY

Lead Contact

Further information and requests for resources and reagents should be directed to and will be fulfilled by the Lead Contact, Dr. Timothy F. Osborne (tosborn9@jhmi.edu).

Materials Availability

Unique reagents generated in this study will be made available on request, but we may require a payment and/or a completed Materials Transfer Agreement.

Data and Code Availability

This study did not generate/analyze datasets/code.

EXPERIMENTAL MODEL AND SUBJECT DETAILS

Animal Experiments

All animal experiments were performed in accordance with accepted standards of animal welfare and with permission of the Sanford Burnham Prebys Medical Discovery Institute at Lake Nona IACUC (protocol 2012-88). 9-13-week old male C57BL/6J mice were obtained from Jackson Laboratory and maintained on a normal chow diet (Teklad Diets, #2016) and housed on a 12-hr light:12-hr dark cycle.

C57BL/6J mice were dosed vehicle or dipyridamole via intraperitoneal (i.p.) administration in fasted or re-fed condition. For fasted group, mice were fasted for 24 hours. During the dark cycle (ZT=16), mice were dosed i.p. with vehicle (50 mg/mL PEG-600 (Sigma-Aldrich, cat# 202401) and 2 mg/mL DL tartaric acid (Sigma-Aldrich, cat# T400)). Fasted mice were euthanized 8 hours after dosing (ZT=0). For re-fed group, mice were fasted for 23 hours, dosed i.p. with vehicle, dipyridamole (120 mg/kg) or modified dipyridamole (referred here as TM-dipyridamole) (120 mg/kg) at ZT=16. 1 hour after dosing, mice were fed a normal chow diet and were sacrificed at ZT=0. Fasted and re-fed mice were euthanized using CO_2 followed by cervical dislocation. Livers were collected for gene expression and protein analyses.

Cell Culture

HeLa, HepG2 and HEK293T cells were cultured in Dulbecco's Modified Eagle's Medium (DMEM) supplemented with 10% (v/v) heat-inactivated fetal bovine serum (FBS) with 100U/mL penicillin/streptomycin (Gibco) at 37°C in an atmosphere of 5% CO_2. In order to

evaluate the effects of dipyridamole and other compounds on SREBP processing, cells were seeded in a 6-well plate format overnight before switching to DMEM supplemented with 5% lipoprotein deficient serum (LPDS) (Sigma-Aldrich) containing sterols (12 ug/mL cholesterol and 1 μg/mL 25-OH cholesterol) (S+) or atorvastatin (10 μM) (S-). Cells were treated with dipyridamole (Tocris), TM-dipyridamole (SBP), PF-07079672 (Pfizer Inc), cycloheximide (CHX) (Cayman Chem), brefeldin A (Sigma-Aldrich), forskolin (Cayman Chem), IBMX (Tocris), 8-pCPT-cGMP (Sigma-Aldrich).

CHO-7 cells (a gift from Drs. Michael Brown and Joseph Goldstein) (Metherall et al., 1989) were grown in 60 mm dishes in Ham's F12:DMEM supplemented with 5% (v/v) LPDS and antibiotics at 37°C in an atmosphere of 5% CO_2. The following day cells were treated with DMSO or dipyridamole (0.3, 1, 3, 10 μM) with or without cholesterol. Cells were re-fed with fresh medium every 2-3 days. After 12 days, CHO-7 cells were washed using cold PBS and fixed using ice-cold 100% methanol. Cells were stained using 0.5% crystal violet. Plates were washed to remove excess crystal violet and dried at room temperature.

METHOD DETAILS

Nuclear Fractionation

Nuclear fraction was prepared following the methods as described previously (Roqueta-Rivera et al., 2016). Briefly, fresh mouse livers were dissected and finely minced using a sharp razor blade. Minced tissues were transferred to a fresh conical tube containing cold phosphate buffered saline (PBS) (137 mM NaCl, 2.7 mM KCl, 8 mM Na_2HPO_4, and 2 mM KH_2PO_4) with 1 mM phenylmethylsulfonyl fluoride (PMSF) (Thermo Fisher Scientific), protease inhibitor cocktail (Sigma-Aldrich), and Halt's phosphatase inhibitor (Thermo Fisher Scientific). Livers were centrifuged 900 × *g* for 5 minutes at 4°C. Liver pellets were Dounce homogenized in homogenization buffer (2 M sucrose, 10% glycerol, 0.15 mM spermine, 25 mM KCl, 1 mM EDTA, 1 mM EGTA, 10 mM HEPES pH 7.6) with protease and phosphatase inhibitors. Homogenized livers were centrifuged at 100,000 × *g* for 1 h at 4°C using SV-40 rotor on Beckman-Coulter Ultracentrifuge. Nuclear pellets were re-suspended in nuclear lysis buffer (50 mM Tris pH 7.6, 500 mM NaCl, 10 mM EDTA) with protease and phosphatase inhibitors. Re-suspended pellets were sonicated using a Bioruptor (Diagenode) and centrifuged 20,000 ×g for 5 minutes at 4°C. Supernatant was collected and transferred to a fresh tube. Protein concentrations were measured using BCA protein assay kit (Thermo Fisher Scientific). Nuclear protein samples were subjected to SDS-PAGE using 7.5% gel and transferred to a nitrocellulose membrane.

Membrane Fractionation

Membrane fraction was prepared following methods as described previously (Engelking et al., 2004) with minor modifications. Briefly, 100mg of frozen liver was transferred to a Dounce homogenizer and homogenized in buffer (20 mM Tris-HCl pH 7.4, 2 mM MgCl2, 0.25 mM sucrose, 10 mM sodium EDTA, and 10 mM sodium EGTA) with 1 mM PMSF (Thermo Fisher Scientific), protease inhibitor cocktail (Sigma-Aldrich), and Halt's phosphatase inhibitor (Thermo Fisher Scientific). Homogenized livers were centrifuged 1,000 × *g* for 5 minutes at 4°C. To collect membrane proteins, supernatants were transferred to a fresh 1.5 mL Beckman tubes (catalog #357448) and centrifuged 100,000 × *g* for 45 minutes at 4°C. The resulting membrane pellets were re-suspended in SDS-containing buffer. Protein concentrations were measured using BCA protein assay kit (Thermo Fisher Scientific). Membrane proteins were diluted with a mixture of urea buffer, sample buffer and β-mercaptoethanol to a final concentration of 2 μg/μL. Membrane protein samples were incubated for 20 minutes at 37°C. Membrane protein samples were subjected to SDS-PAGE using 10% gel and transferred to a nitrocellulose membrane.

Modification of Dipyridamole

A modified dipyridamole was synthesized following previously reported chemical reactions (Curtin et al., 2004; Lin and Buolamwini, 2007). To synthesize a modified dipyridamole molecule (N2,N2,N6,N6-tetrakis(2-methoxyethyl)-4,8-di(piperidin-1-yl)pyrimido[5,4-d]pyrimidine-2,6-diamine (TM-Dipyridamole, compound **2** below), dipyridamole (compound **1** below, 120 mg, 0.238 mmol) was dissolved in 3.3 mL of N,N-dimethylformamide and treated with 60% sodium hydride (71 mg, 1.77 mmol). The vessel was swept with nitrogen, wrapped in foil, and maintained under nitrogen with stirring. After one hour, iodomethane (0.67 mL, 45 mmol) was added and the mixture was stirred under nitrogen at room temperature. After 4 hours, analysis by LCMS suggested good conversion and the reaction was quenched with 1 mL of water, diluted with an additional 30 mL of water, and then extracted with two 25 mL portions of methylene chloride. The organics were dried over magnesium sulfate and concentrated to 173.8 mg of crude product, a yellow film which was purified by flash chromatography (30 mL of silica gel, eluting with 10% acetone in hexane) to return 112 mg (84%) of **2**, a yellow powder.

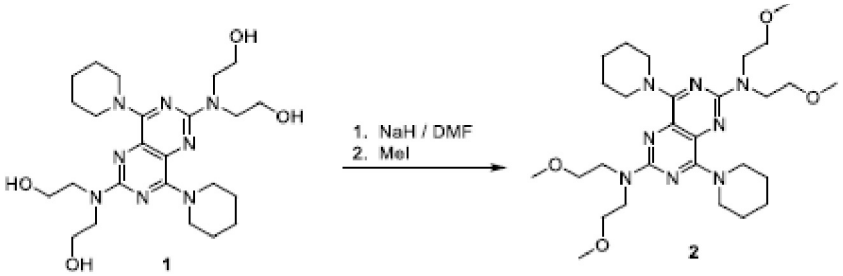

Lipid Dependent Growth Assay

Lipid dependent growth assay was performed using CellTiter 96 Aqueous One Solution Cell Proliferation Assay kit (Promega) as described previously (Shao et al., 2016). Briefly, cells were seeded at a density of 5×10^3 cells per well (96-well plate) in conditions indicated in figure legends. 72 hours later, MTS (15 μl per well) was added, incubated at 37°C for 3 hours, then A_{570} was measured. Viability was normalized to vehicle-treated condition and plotted by GraphPad (log(inhibitor) vs. response – variable slope, 4 parameters).

VSVG Maturation Assay

Vesicular stomatitis virus G (VSVG) protein maturation was measured as described previously (Shao et al., 2016). Briefly, CHO-7 cells were plated at 1×10^5 cells per well (in 24-well plate format) the day before the experiment. At Time 0, cells were infected by VSV (San Juan strain, Indiana serotype) (Cluett et al., 1997) at a multiplicity of infection (MOI) of 10 for 30 min. Then infection medium was replaced by Medium A (DMEM/F-12 (1:1) containing 100 units/mL penicillin and 100 μg/mL streptomycin sulfate supplemented with 5% (v/v) fetal bovine serum (FBS)), and cells were incubated for 2.25 hours. At T=2.75 hr., for vehicle and TM-dipyridamole-treated wells, cells were incubated in Medium A containing either vehicle (0.1% DMSO) or TM-dipyridamole (3 μM) respectively, for 45 min. At T=3.5 hr., cells were starved in serum-, cysteine-, and methionine-free DMEM containing either vehicle (0.1% DMSO), TM-dipyridamole (3 μM) or brefeldin A (3 μg/mL) for 15 min before labeling for 15 min with 0.5 ml of serum-, cysteine-, and methionine-free DMEM containing 200 μCi/ml l-[^{35}S] *in vitro* cell labeling mix (Amersham, Arlington Heights, IL) containing either vehicle (0.1% DMSO), TM-dipyridamole (3 μM) or brefeldin A (3 μg/ml). At T=4 hr., cells were chased for indicated time (20, 40 and 60 min) in Medium A supplemented with 5% (v/v) FBS with vehicle (0.1% DMSO), TM-dipyridamole (3 μM) or brefeldin A (3 μg/ml). Cells were lysed in detergent solution (50 mM Tris, pH 8.0, 1% NP-40, 0.4% deoxycholate, and 2.5 mM EDTA) with 20 μg/ml aprotinin, 20 μg/ml leupeptin, and 2 μg/ml pepstatin A, and an aliquot was directly treated with endoglycosidase H (0.4mU; New England Biolabs, Beverly, MA) after denaturation. Proteins were separated on 4-12% Bis-Tris polyacrylamide gels (NUPAGE, Invitrogen) and detected using a Molecular Imager FX PhosphorImager (Bio-Rad). The percent of protein processed at each chase time was determined after quantitation using Quantity One software (Bio-Rad)

Transfection

Cells were transfected using Lipofectamine 2000 (Thermo Fisher Scientific) with the following plasmids: pQCXIN-3xFLAG-pSREBP-1a, pQCXIN-3xFLAG-pSREBP-1c (Wu et al., 2014), pQCXIN-3xFLAG-pSREBP-2 (gifts from Dr. Jared Rutter), pcDNA3.1-2xFLAG-nSREBP-2 (Toth et al., 2004), pcDNA3.0-GFP-SCAP (Nohturfft et al., 2000), pCMV-S1P-Myc-KDEL (DeBose-Boyd et al., 1999) (gift from Dr. Russell DeBose-Boyd), and pCMV-Insig-1-6xMyc (ATCC). HeLa cells were co-transfected with pQCXIN-3xFLAG-pSREBP-2 plasmid and pooled siRNAs against INSIG1 and INSIG2 (GE Healthcare) using Lipofectamine 2000 (Thermo Fisher Scientific).

Co-immunoprecipitation

HeLa cells were transfected with pCMV-INSIG-1-6xMyc and pCMV-GFP-SCAP using Lipofectamine 2000 (Thermo Fisher Scientific) in DMEM supplemented with 10% (v/v) heat inactivated FBS without antibiotics at 5% CO_2, 37°C. Cells were incubated in DMEM supplemented 5% (v/v) LPDS (Alfa Aesar) and 1% HPCD (Sigma-Aldrich) for 1 hour. Cells were washed, incubated in DMEM supplemented with 5% LPDS and 1% HPCD, and treated with vehicle or dipyridamole for 6 hours. Cells were lysed in IP lysis buffer (50 mM HEPES pH 7.6, 100 mM NaCl, 1.5 mM MgCl2, and 0.1% IGEPAL) containing 1 mM PMSF (Thermo Fisher Scientific), protease inhibitor cocktail (Sigma-Aldrich) and Halt's phosphatase inhibitor (Thermo Fisher Scientific). Cells were homogenized by passing through a 23-gauge needle syringe 20 times. Cell lysates were centrifuged 17,000 × *g* for 20 minutes at 4°C. Supernatant was collected to measure protein concentration using BCA protein assay kit (Thermo Fisher Scientific). ~600 μg of protein was used for immunoprecipitation using an antibody against Myc (SCBT, cat# sc-40) conjugated to Dynabeads Protein G magnetic beads (Thermo Fisher Scientific). Proteins bound to magnetic beads were denatured using a denaturing buffer (10 mM Tris HCl pH 7.4, 100 mM NaCl, 1% SDS) with sample buffer and β-mercaptoethanol. Magnetic beads were boiled for 5 minutes at 95°C and allowed to interact with the magnet for 1 minute before centrifugation. The supernatant was collected and used for immunoblotting.

Immunoblotting

Nuclear and membrane protein fractions were prepared as described above. To prepare whole cell lysates, HeLa cells were lysed using RIPA buffer (50 mM Tris-HCl, pH 8.0, 150 mM NaCl, 1% IGEPAL, 0.5% w/v sodium deoxycholate and 0.1% w/v sodium dodecyl sulfate) with 1 mM PMSF (Thermo Fisher Scientific), protease inhibitor cocktail (Sigma-Aldrich) and Halt's phosphatase inhibitor (Thermo Fisher Scientific). Protein samples were subjected to 7.5% and 10% SDS-PAGE gels, after which were transferred to nitrocellulose membranes.

Nitrocellulose membranes were incubated overnight with primary antibodies against SREBP-1 (ATCC, catalog # CRL-2121), SREBP-2 (Seo et al., 2011), SCAP (SCBT, catalog # sc-13553), Insig-2 (Hegarty et al., 2005) (gift from Dr. Fabienne Foufelle), FLAG (Sigma, catalog # F1804), Myc (SCBT, catalog # sc-40), phospho-PKA substrate (RRXS*/T*) (Cell Signaling, catalog # 9624), phospho-AKT (Ser473) (Cell Signaling, catalog #4060), phospho-AKT (Thr308) (Cell Signaling, catalog # 13038), total AKT (Cell Signaling, catalog # 4685), phospho-S6 ribosomal protein (Cell Signaling, catalog # 5364), total S6 ribosomal protein (Cell

Signaling, catalog # 2217), β-actin (Sigma, catalog# A2228), calnexin (Abcam, catalog # ab22595) and YY-1 (SCBT, catalog# sc-7341).

Bound antibodies were visualized by chemiluminescence (SuperSignal Substrate; Thermo Scientific) using secondary antibodies conjugated to horseradish peroxidase, or by fluorescence (ECF Substrate; GE Healthcare Life Sciences) using a secondary antibody conjugated to alkaline phosphatase (Sigma-Aldrich). Immunoblot intensities were quantified using ImageQuant (GE Healthcare Life Sciences).

Immunostaining

HeLa cells were seeded in Lab-Tek chamber slides (Thermo Fisher Scientific) in DMEM supplemented with 10% (v/v) FBS and 100 U/mL penicillin/streptomycin (Gibco) and allowed to attach to slides overnight. HeLa cells were serum starved by incubating in DMEM supplemented with 5% LPDS overnight at 37°C in an atmosphere of 5% CO_2. The following day, HeLa cells were switched to DMEM supplemented with 5% LPDS containing sterols (12 ug/mL cholesterol, 1 ug/mL 25-OH cholesterol) or atorvastatin (10 uM) with DMSO or dipyridamole. After 6 hours, cells were washed using cold 1x PBS, fixed using 4% paraformaldehyde. For SREBP-2 immunostaining, fixed cells were incubated in a solution consisted of polyclonal antibody against SREBP-2 raised in rabbit and diluted in 5% normal goat serum (NGS) (Vector Laboratories) in phosphate-buffered saline with 0.05% Triton X-100. A donkey anti-rabbit Alexa Fluor 488 (Thermo Fisher Scientific) secondary antibody diluted in 5% NGS buffer was used to detect SREBP-2.

CHO/pGFP-SCAP cells (Nohturfft et al., 2000) were seeded in Lab-Tek chamber slides (Thermo Fisher Scientific) in Ham's F-12:DMEM medium supplemented with 10% (v/v) fetal calf serum and 100 U/mL penicillin/streptomycin (Gibco) and allowed to attach to slides overnight at 37°C in an atmosphere of 5% CO_2. The following day, CHO/pGFP-SCAP cells were switched to Ham's F-12:DMEM medium supplemented with 5% LPDS, 1% hydroxypropyl-β-cyclodextrin (HPCD) with sterols or dipyridamole. After 6 hours, cells were fixed and stained using a rabbit antibody against RCAS1 (Cell Signaling). To visualize RCAS1 localization, a Cy5-conjugated goat anti-rabbit secondary antibody (Thermo Fisher Scientific) was used.

Slides were mounted using ProLong Gold Mountant (Thermo Fisher Scientific). Slides were dried in the dark at room temperature before imaging. Immunofluorescence images were captured using an A1R confocal microscope (Nikon Instruments). Pearson's correlation coefficients were measured from stacked images of 100 cells/group using Volocity software (PerkinElmer).

PDE5A Phosphodiesterase Inhibitor Assay

The PDE5A1 Assay kit (BPS Biosciences) was used to evaluate phosphodiesterase (PDE) inhibition of dipyridamole and TM-dipyridamole according to the manufacturer's instructions. Briefly, all test compound stocks solutions (500 mM IBMX; 10 mM dipyridamole; 10 mM TM-dipyridamole) were prepared in 100% DMSO and subsequently diluted to 10x working stock concentrations in 10% dimethyl sulfoxide (DMSO) in the PDE assay buffer included in the kit (500 μM IBMX; 30 μM and 100 μM dipyridamole; 30 μM and 100 μM TM-dipyridamole). A final concentration of 1% DMSO was present in each PDE5A1 enzyme inhibition reaction, including the PDE5A1 positive control reaction. Based on preliminary tests, concentrations greater than 1% DMSO negatively-affected the PDE5A1 enzymatic activity (data not shown). The fluorescent polarization of each sample was analyzed using a PerkinElmer EnVision 2105 Multimode Plate Reader equipped with a FITC FP 480 nm excitation filter and emission filters FITC FP P-pol 535 nm and FITC S-pol 535 nm. Milli-polarization values (mP) were calculated with the EnVision Workstation v1.12 software and PDE5A1 enzymatic activity for each reaction was normalized to the enzymatic positive control sample.

Click Chemistry

HEK293T cells were co-transfected with pCMV-INSIG-1-6xMyc and pGFP-SCAP plasmids and incubated overnight in antibiotic-free and serum-free medium (DMEM supplemented with 5% LPDS and atorvastatin (10 μM)). The following day, cell culture medium was replaced with 10 mL serum-free medium containing vehicle (0.1% DMSO) or 20 μM TM-dipyridamole (competitor compound) was added, and cells were incubated for 1 hour at 37°C, 5% CO_2. Without replacing medium, clickable photoprobe PF-07079672 (0.1 μM) was then added, and incubated for 1 hour at 37°C, 5% CO_2. Cells underwent UV irradiation (365 nM for 10 minutes in 4°C). After UV irradiation, plates were washed with cold 1x PBS, and harvested with a cell scrapper. Cell suspensions were centrifuged at 10,000 × *g* for 2 minutes in 4°C to collect cell pellets. Cell pellets were resuspended in 500 μL 1x PBS and sonicated on ice. Protein concentrations determined using BCA assay and adjusted protein concentration of each sample to 2 mg/ml. 500 μL of each sample were subjected to Cu(I)-catalyzed azide-alkyne cycloaddition (CuAAC) as described previously (Xu et al., 2019). Briefly, 34 μL of 1.7 mM TBTA in DMSO:t-BuOH (v:v 1:4), 11.3 μL of 50 mM CuSO4 in water, 11.3 μL of 50 mM freshly prepared TCEP in water, and 2.3 μL of 50mM biotin rhodamine azide (Huang et al., 2019) in DMSO, were prepared and then added to each sample. Mixture was incubated at room temperature for 1 hour with mild agitation. Samples were cooled and transferred to fresh 15 mL conical tubes, and proteins were precipitated by adding 2 mL ice-cold MeOH. 500 μL of cold $CHCl_3$ was added to samples and vortexed. This was followed by adding 1 mL cold 1x PBS to samples and mixed by vortexing. Samples were centrifuged at 5000 × *g* for 10 minutes for phase separation. The protein discs were washed carefully with 1:1 (v/v) MeOH:$CHCl_3$ (3 x 1 mL), sonicated in 2 mL MeOH and 500 μL $CHCl_3$ was added. Protein was pelleted by centrifugation at 5000 × *g* for 10 minutes and air dried for 5 minutes. Protein pellets were re-suspended in 160 μL 10% SDS. 500 μL 50 mM Tris buffer (pH 8.0) was added to samples followed by sonication. Samples were further diluted in 11 mL 50mM Tris buffer (pH 8.0). For pull down assay, 50 μL of high capacity Streptavidin agarose resin beads (Pierce) were added and incubated overnight at 4°C. The resin was pelleted by centrifugation at 1,500 × *g* for 3 minutes, washed with 0.1% SDS/50mM Tris (3 x 10 mL) and twice with 10 mL of 50 mM Tris buffer (pH 8.0). Proteins bound to Streptavidin agarose beads

were denatured in Laemmli sample buffer with β-mercaptoethanol. Agarose beads were boiled at 95°C for 5 minutes. Samples were centrifuged at 10,000 × *g* for 1 minute. Supernatant was collected and used for immunoblotting.

RNA Isolation and Gene Expression Analysis

Total RNA was prepared from mouse livers and cells using Direct-zol RNA miniprep kit (Genesee Scientific) following manufacturer's protocol. Briefly, ~50 mg of mouse livers were transferred into fresh 2 mL tubes with glass beads. Tissues were homogenized in TRIzol (Thermo Fisher Scientific) using Geno/Grinder tissue homogenizer (Spex Sample Prep). To isolate total RNA from HeLa cells, cells were lysed in TRIzol. RNA concentrations were measured using NanoDrop. 1 μg of total RNA was converted into cDNA using iScript cDNA synthesis kit (Bio-Rad). Specific primers for each gene were designed using Primer Blast (NCBI resources). To measure relative gene expression, SYBR green RT-qPCR assay was performed using specific forward and reverse primers for genes of interest and 2x SsoFast Evagreen Supermix (Bio-Rad). qPCR reactions were performed using the Bio-Rad CFX96 Real-Time PCR Detection System. Relative mRNA expression levels were calculated using the comparative threshold cycle (C_T) method and normalized to mouse L32 or human GAPDH mRNA expression (Table S1).

QUANTIFICATION AND STATISTICAL ANALYSIS

Pearson's correlation coefficient values for GFP-SCAP and RCAS1 co-localization (n=100 cells/condition) were measured using Volocity software (Perkin-Elmer). All data are presented as mean ± SEM, as described in the figure legends. Differences between the means of the individual groups were assessed by Student's t-test. Differences were considered significant at p-value < 0.05. The statistical software package Prism 8.0 (GraphPad) was used for analysis.